Climate Dynamics (2019) 53:405–426
https://doi.org/10.1007/s00382-018-4590-8

New insights into the rainfall variability in the tropical Andes on seasonal and interannual time scales

Hans Segura[1] · Clementine Junquas[1] · Jhan Carlo Espinoza[1,2] · Mathias Vuille[3] · Yakelyn R. Jauregui[4] · Antoine Rabatel[1] · Thomas Condom[1] · Thierry Lebel[1]

Received: 27 February 2018 / Accepted: 17 December 2018 / Published online: 2 January 2019

Abstract

In this study, we analyze the atmospheric mechanisms associated with the main rainfall patterns in the tropical Andes (20°S–1°N) on seasonal and interannual time scales. Using a homogeneous and high spatial resolution precipitation data set (0.05° × 0.05°) at monthly time step (CHIRPS; 1981–2016), in-situ precipitation from 206 rain-gauge stations, power spectrum and EOF analysis, we identify three Andean regions characterized by specific seasonal and interannual rainfall modes: the equatorial Andes (EA, 5°S–1°N), the transition zone (TZ, 8°S–5°S) and the southern tropical Andes (STA, 20°S –8°S). On seasonal time scales, the main mode of precipitation in the EA and STA are characterized by a unimodal regime, while the TZ is represented by a bimodal regime. The EA and the TZ share the same wet season in the February–April period, which is associated with a weakened Walker Cell, the southerly position of the Intertropical Convergence Zone (ITCZ) and a strong westward humidity transport from the equatorial Amazon. This latter mechanism and a reduced elevation of the Andes are associated with the October–November wet season in the TZ. The presence of the Bolivian High and the northward extension of the Low Level Jet are associated with the precipitation over Andean regions between 20°S and 8°S in the December–March period. On interannual time scales, extreme monthly wet events (EMWE) in the STA (TZ) are related to convection over the western (equatorial) Amazon during the December–March (February–April) period, showing an atmospheric relationship between the Amazon and the Andes. Extreme monthly dry events (EMDE) in the TZ and in the EA during the February–April period are related to a strengthened Walker Cell, especially in the eastern Pacific. In addition, EMWE (EMDE) in the EA are associated with an anomalous southward (northward) displaced eastern Pacific ITCZ. Moreover, we find a relationship between precipitation at higher elevations in the Andes north of 10°S and easterly winds at 200 hPa during February–April EMWE. Finally, extreme monthly events in the EA (STA) are related to sea surface temperature anomalies in the western (central) equatorial Pacific.

Keywords Tropical Andes · Precipitation · EOF analysis · Atmospheric mechanisms · Seasonal and interannual variability

1 Introduction

The Andes are the largest mountain chain in the world, extending South–North over 7240 km from Patagonia to Venezuela, and the highest mountain chain situated in the inner tropics. Over the south tropical and equatorial region the Andes act as a topographic barrier between the cold and dry eastern Pacific and the warm and moist Amazon region, which produces a strong zonal gradient of precipitation (Fig. 1a, b; e.g. Bendix and Lauer 1992; Garreaud 1999; Houston and Hartley 2003; Garreaud 2009; Espinoza et al. 2015). The complexity of the topography and the low density of the rainfall network over these Andean regions have complicated the proper characterization of the spatio-temporal

Electronic supplementary material The online version of this article (https://doi.org/10.1007/s00382-018-4590-8) contains supplementary material, which is available to authorized users.

✉ Hans Segura
hans.segura@univ-grenoble-alpes.fr

[1] Univ. Grenoble Alpes, IRD, CNRS, G-INP, IGE (UMR 5001), 38000 Grenoble, France

[2] Instituto Geofísico del Perú (IGP), Lima, Peru

[3] Department of Atmospheric and Environmental Sciences, State University of New York at Albany, Albany, NY, USA

[4] Department of Atmospheric Sciences, University of Washington, Seattle, USA

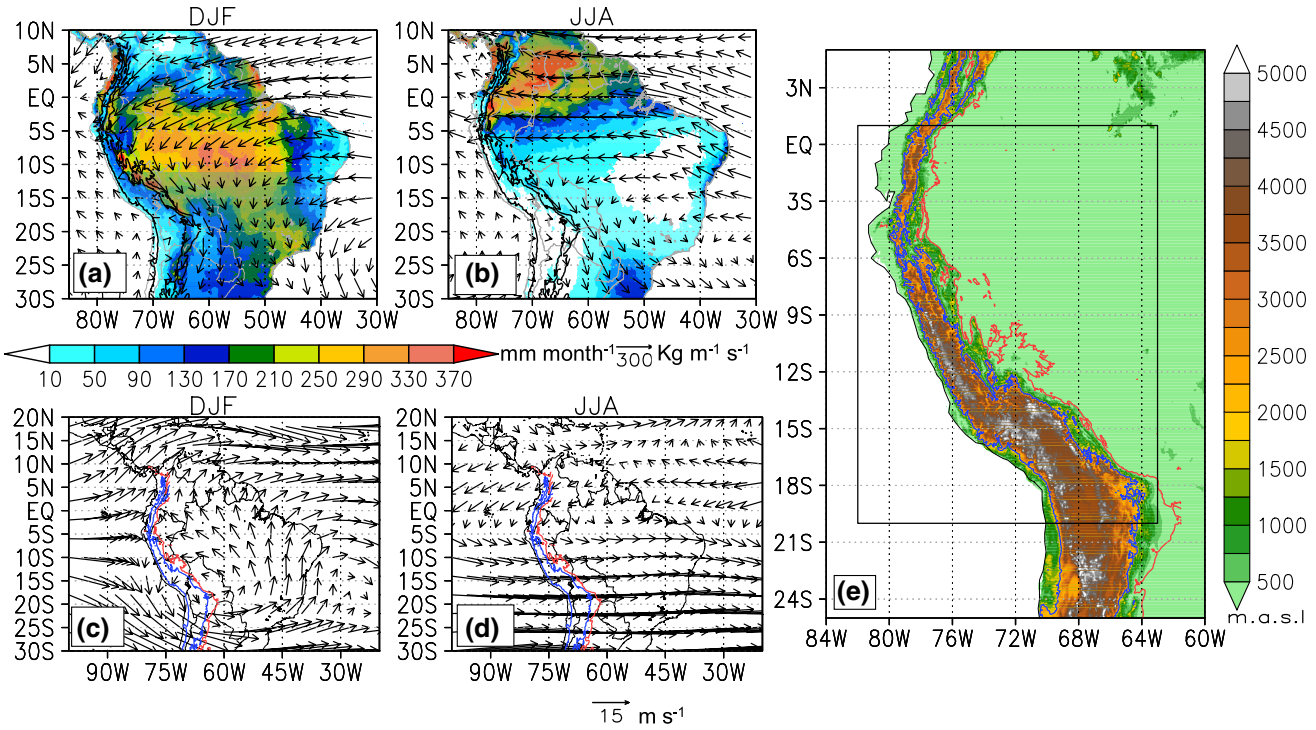

Fig. 1 Average CHIRPS precipitation (shaded) and vertically integrated water vapor flux (vectors) from **a** December to February (DJF), **b** June to August (JJA). Average wind field at 200 hPa (vectors) is displayed for **c** DJF and **d** JJA. **e** Topographic map (shaded) of western South America using 30 m—resolution SRTM data and the region of study (black rectangle). The contour line of 2000 m.a.s.l is plotted for the eastern and western side of the Andes, while the line at 350 m.a.s.l is only plotted in the eastern region in **a**, **b** as black solid line. In **c**–**e** the altitude of 350 m.a.s.l is plotted as a red line and the altitude of 2000 m.a.s.l as a blue line

patterns of precipitation. In this study we will focus on the precipitation variability over the south tropical and equatorial Andes on seasonal and interannual time scales.

On seasonal time scales, rain-gauge stations over the southernmost tropical Andes have shown the presence of an unique wet period in the austral summer (December–February; Vuille and Keimig 2004; Garreaud 2009). This seasonal peak of precipitation is related to the mature phase of the South American Monsoon System, which is associated with the presence of both the Low Level Jet (LLJ) and the Bolivian High (BH) in the lower and upper troposphere of western South America, respectively (Fig. 1a, c; e.g. Horel et al. 1989; Zhou and Lau 1998; Vera et al. 2006; Garreaud et al. 2009). Studies have shown that the wet season over the southern tropical eastern Andes / western Amazon region (350–2000 m.a.s.l.), known as "hotspot" precipitation regions, is associated with the northernmost position of the LLJ (Espinoza et al. 2015; Junquas et al. 2016; Chavez and Takahashi 2017). On the other hand, the seasonal peak of precipitation at higher elevations in the southern tropical Andes (> 3000 m.a.s.l.), especially over the Altiplano (22° S–15°S), is related to the presence of the BH (Virji 1981; Vuille et al. 1998; Garreaud 1999; Garreaud et al. 2003; Vuille and Keimig 2004; Garreaud 2009). However, the latitudinal extension of this rainfall regime and the influence of the LLJ and BH over the tropical Andes during the wet season have not been investigated in previous studies. It is thus one of the principal objectives addressed in this study.

Over the equatorial Andes, rain-gauge stations display a more complex seasonal rainfall variability than the southern tropical Andes (Bendix and Lauer 1992; Laraque et al. 2007; Espinoza et al. 2009; Rollenbeck and Bendix 2011; Campozano et al. 2016, 2018). The eastern slope presents a unimodal regime with a peak in the June–August period, which is associated with an intensification of the westward humidity transport from the equatorial Amazon and orographic uplift forced by the topography of the Andes (Bendix and Lauer 1992; Rollenbeck and Bendix 2011; Campozano et al. 2016). The high equatorial Andes are characterized by two rainfall seasons: one in the February–April period and the second one in the October–December period (Bendix and Lauer 1992; Laraque et al. 2007; Espinoza et al. 2009; Rollenbeck and Bendix 2011; Campozano et al. 2016, 2018). Bendix and Lauer (1992) argued that the rainfall in the February–April period is related to atmospheric processes of the eastern Pacific region and winds from the Panama Gulf. In contrast, the atmospheric mechanisms associated with the rainfall in the October–December period have not been

thoroughly studied. Moreover, the non-homogeneous spatial distribution of rain-gauge stations over this region has complicated the task to characterize properly the zones where the unimodal or bimodal rainfall regimes dominate.

In contrast to the seasonal variability, the interannual precipitation variability in the upper-elevation zone of the southern tropical Andes has been studied using rain-gauge stations and satellite data sets (e.g. Vuille 1999; Garreaud 1999; Vuille and Keimig 2004; Sulca et al. 2018). Results indicate that precipitation in this region responds principally to the sea surface temperature (SST) variability in the central Pacific Ocean and to zonal winds in the upper troposphere of the southern tropical Andes, which is a proxy of the position and strength of the BH. (e.g. Vuille 1999; Garreaud 1999; Garreaud et al. 2003; Vuille and Keimig 2004; Vuille et al. 2008; Lagos et al. 2008; Lavado and Espinoza 2014; Sulca et al. 2018; Rau et al. 2017). A weak (strong) and northward (southward) displaced BH is associated with westerly (easterly) anomalies at 200 hPa over the southern tropical Andes, which inhibits (enhances) moisture influx from the east, thereby increasing (reducing) atmospheric stability and reducing (increasing) precipitation over upper-elevation regions of the Andes (Garreaud 1999; Garreaud et al. 2003; Vuille and Keimig 2004). Besides, westerly (easterly) anomalies at 200 hPa over the southern tropical Andes are strongly associated with warm (cold) SST anomalies in the central Pacific. Sulca et al. (2018) demonstrated that the low precipitation values in the hotspot precipitation regions are also related to warm SST anomalies in the central Pacific. Therefore, this could suggest a relationship between the precipitation over the western Amazon and over the upper-elevation zones in the southern tropical Andes, which has not been fully studied before on interannual time scales.

Similarly to what is observed on seasonal time scales, rain-gauge stations over the equatorial Andes show a complex spatial precipitation variability on interannual time scales. Precipitation over the western region is related to the SST over the central and eastern tropical Pacific while rainfall over the eastern region is associated with SST anomalies in the tropical Atlantic Ocean (Vuille et al. 2000; Francou et al. 2004; Lagos et al. 2008; Bendix and Bendix 2006; Vicente-Serrano et al. 2017; Campozano et al. 2018; Tobar and Wyseure 2018). Recent studies using in-situ and satellite precipitation data sets demonstrated that warm SST anomalies in the central Pacific Ocean are related to less precipitation in the upper-elevation equatorial Andes, whereas a warming in the eastern Pacific triggers convection and precipitation over western slopes of the equatorial Andes during the austral summer (December–February; Bendix and Bendix 2006; Lavado and Espinoza 2014; Sulca et al. 2018; Vicente-Serrano et al. 2017; Tobar and Wyseure 2018). Unlike the situation in the southern tropical Andes, no significant relationship between austral summer precipitation and wind field at 200 hPa over the equatorial Andes has been observed (Francou et al. 2004; Sulca et al. 2018). Despite the fact that the February–April period is the wettest season in most of the equatorial Andes, the interannual precipitation variability in this period and its associated atmospheric mechanisms are still not completely understood.

As discussed above, the equatorial and southern tropical Andes display a complex spatio-temporal precipitation pattern, shaped by a unique geographic configuration. The difficult access to large areas is one of the factors responsible for the poor density of the rain-gauge network covering this region, which hitherto has limited the ability of the scientific community to characterize the rainfall regime and its links to atmospheric circulation and SST fields in more detail. New satellite data sets are now documenting precipitation at high spatial resolution over more than three decades. Combining various data sets described in Sect. 2 (CHIRPS for precipitation, ERA-Interim for the atmospheric dynamics and ERSST V.4 for SST) allows us to address two major issues in this paper: (1) obtaining a refined vision of the rainfall regimes over the entire southern hemisphere range of the tropical Andes (20°S–1°N; Fig. 1e), focusing on the seasonal cycle and how it varies from the southern tropical to the equatorial region as well as on the interannual time scales (Sect. 3); (2) studying the physical processes associated with these patterns for both the seasonal cycle (Sect. 4) and the interannual variability (Sect. 5). A summary and discussion of our findings are given in Sect. 6.

2 Data and methods

2.1 Data

Satellite precipitation The Climate Hazards group Infrared Precipitation with Stations (CHIRPS; Funk et al. 2015) was used to analyze the spatial and temporal precipitation variability in the equatorial and southern tropical Andes. CHIRPS merges satellite products with gauge stations to produce a high spatial resolution rainfall product ($0.05° \times 0.05°$; Fig. 1a, b), useful for the analysis of precipitation in regions with complex topography, such as the Andes. We used data for the period from January 1981 to December 2016 at a monthly time step.

In-situ precipitation With the aim of comparing our results using CHIRPS, we used in-situ precipitation from rain-gauge stations located in Peru and Ecuador. The precipitation data set was obtained from the Peruvian National Service of Meteorology and Hydrology (SENAMHI) and the Ecuadorian National Institute of Meteorology and Hydrology (INAMHI). We made used of monthly precipitation data from 184 (22) rain-gauge stations located over the Peruvian (Ecuadorian) Andes over the period 1970–2013

(1982–2009). The monthly missing values (< 20%) were not been replaced. The detailed information regarding the rain-gauge stations (name, longitude, latitude and altitude) are given in Table S1.

Atmospheric variables In order to identify the main atmospheric circulation patterns associated with precipitation in our study region, we used the 38-year reanalysis data set ERA-Interim (0.5° × 0.5°; January 1981–December 2016) from the European Centre for Medium-Range Weather Forecasts (ECMWF) at monthly time step (Dee et al. 2011). Specifically we used the vertically integrated water vapor flux and the vertically integrated tropospheric water vapor, downloaded from http://apps.ecmwf.int/datasets/data/interim-full-moda/levtype=sfc/. The horizontal and vertical components of wind, the potential temperature and the specific humidity were used globally at pressure levels between 1000 and 100 hPa. In addition, using the horizontal wind at 200 hPa, we computed the 200 hPa divergent wind with the objective of relating large-scale subsidence and deep convection with precipitation variability in the tropical Andes, as computed in previous papers (e.g. Krishnamurti et al. 1973; Tanaka et al. 2004).

Global sea surface temperature We used the Extended Reconstructed Sea Surface Temperature data set (ERSST v.4; Huang et al. 2015) provided by the NOAA/OAR/ESRL PSD, Boulder, Colorado, USA (http://www.esrl.noaa.gov/psd/) for the 1981–2016 period. The spatial resolution is 2.5° × 2.5° with a monthly time step.

2.2 Methods

Delimiting the area of study We used the Shuttle Radar Topography Mission (SRTM) 30 m topography data (https://earthexplorer.usgs.gov/) to delimit the area of analysis, which comprises the equatorial and southern tropical Andes (20°S–1°N). First, for each 0.05° latitudinal band we identified the westernmost grid point with a 2000 m.a.s.l altitude, and then, between the highest altitude of the Andes and the Amazon region, we selected the easternmost altitude of 350 m.a.s.l. Finally, the grid points inside these two limits, referred to as tropical Andes, were used as the study region for the Empirical Orthogonal Function (EOF) Analysis (Fig. 1e). Zones above 2000 m.a.s.l are referred as the upper-elevation Andean region, and zones between 350 and 2000 m.a.s.l, which includes the Andes–Amazon transition region, as the eastern Andean slopes.

Previous studies have shown that positive anomalies of precipitation over the dry western Andean slope region (500–2000 m.a.s.l) are related to strong ENSO warm events, such as in 1982/83 and 1997/98 (Lagos et al. 2008; Lavado and Espinoza 2014; Rau et al. 2017). As our objective is to analyze the precipitation variability over the tropical Andes without assuming a priori relationships with extreme ENSO events, we decided not to include this region in our analysis.

Empirical orthogonal function We used the Empirical Orthogonal Function method (Lorenz 1956) to identify the main spatial modes of precipitation variability in the tropical Andes (EOF's) and their associated temporal variability or principal component (PC's). We used the normalized values of precipitation with the purpose of avoiding any influence of the quantity of precipitation when calculating the PC's. The normalization was done using the following equation:

$$zP_{(i,j,t)} = \frac{P_{(i,j,t)} - \overline{P}_{i,j}}{\sigma(P_{i,j})}, \tag{1}$$

in which $zP_{i,j,t}$ is the normalized precipitation at longitude i, latitude j and time t; $P_{i,j,t}$ is the precipitation at the same grid point (i,j) and time (t); $\overline{P}_{i,j}$ and $\sigma(P_{i,j})$ are the historical mean and standard deviation, respectively of the precipitation at the grid point i,j. As described in the data section (see Sect. 2.1), we used the CHIRPS precipitation data set at monthly time step from January 1981 to December 2016. This means that the seasonal cycle of precipitation at each grid point is not removed since we wanted to jointly analyze the seasonal and the interannual precipitation variability. First, we calculated the principal components (PCs) of the precipitation in a selected Andean region using the singular value decomposition. Secondly, the spatial structures (EOFs) were computed using a correlation analysis between the PC's and the normalized precipitation at each grid point of the tropical Andes, using Eq. 1. Because of the strong autocorrelation in each PC and in the precipitation field due to the intrinsic annual cycle, degrees of freedom were calculated using the methodology proposed by Bretherton et al. (1999) in order to determine correlation coefficients with a significance level of 99% (p-value of 0.01). Moreover, the significance of all the correlation analyses done in this study was also computed using the method of Bretherton et al. (1999).

Cramér test The Cramér method is a statistical test that is used to determine if a portion of a time series has a significantly different mean value compared with the mean value of the total time series (Cramér 1999). It thus serves the same purpose as a Student-t test, except that it allows for the two series to be of different length. It is used here for the composite analysis of atmospheric variables and SSTs with a threshold p-value of 0.05.

Power spectral density We used the power spectral density method in order to identify the Andean regions where either a unimodal or a bimodal annual precipitation regime dominates. First, monthly precipitation at each grid

point in the tropical Andes was detrended and normalized with respect to the historical mean and standard deviation, following Eq. 1. Then, using the Thomson method (Thomson 1982) we calculated the power spectrum density of precipitation at each grid point. The Thomson method uses a finite number of tapers or windows that are created using discrete prolate spheroidal sequences (DPSS), which are orthogonal between them. This means that while the first DPSS increases the weight for the central part of the time series, the second gives more weight to the beginning and the end of the time series. In addition, this implies that for each DPSS a periodogram is estimated. Then, all these periodograms are averaged to create one representative periodogram of the time series. This method ensures that the resulting periodogram is influenced by recurring events rather than single events that occur during a short period of time. In our analysis we used nine (9) DPSS and the periodogram in each grid point has 256 values. In order to identify significant periods, we calculated the red noise (Rn) of the time series with a significance level of 95% (p-value of 0.05). Rn was calculated using the equation provided by Gilman et al. (1963):

$$Rn = \frac{1 - p^2}{1 - 2 \times p \times cos(\frac{\pi \times fr}{fnyq}) + p^2} \quad (2)$$

where p is the one-lag autocorrelation of the time series, fr is the frequency estimated in our periodogram and fnyq is the Nyquist frequency, which is the half of the sampling rate. The Nyquist frequency in our study is 0.5 since the sampling rate is one (1) month. As our objective is to explain the seasonal variability, we only used significant spectrum values between frequencies of 0.2 (5 months) and 0.06 (16.67 months).

The maximum spectral value between 10 and 16.67 months is defined as the unimodal index (PSD_{12}) and the value between 5 and 8 months as the bimodal index (PSD_6). We used the unimodal and bimodal indices in the next equation to estimate the relative difference between the unimodal and bimodal regime (PSD_{12-6}):

$$PSD_{12-6}\% = \frac{PSD_{12} - PSD_6}{PSD_{12}} \times 100\% \quad (3)$$

Negative values of PSD_{12-6} indicate regions with a dominant bimodal regime of annual precipitation, while positive PSD_{12-6} values characterize regions with a predominance of a unimodal regime (Fig. 2a). Values near 0% indicate that unimodal and bimodal regimes have a similar importance in terms of seasonal variability.

Harmonic analysis Missing data is a constant problem when studying the precipitation variability over the tropical Andes and most of the rain-gauge stations used in this study

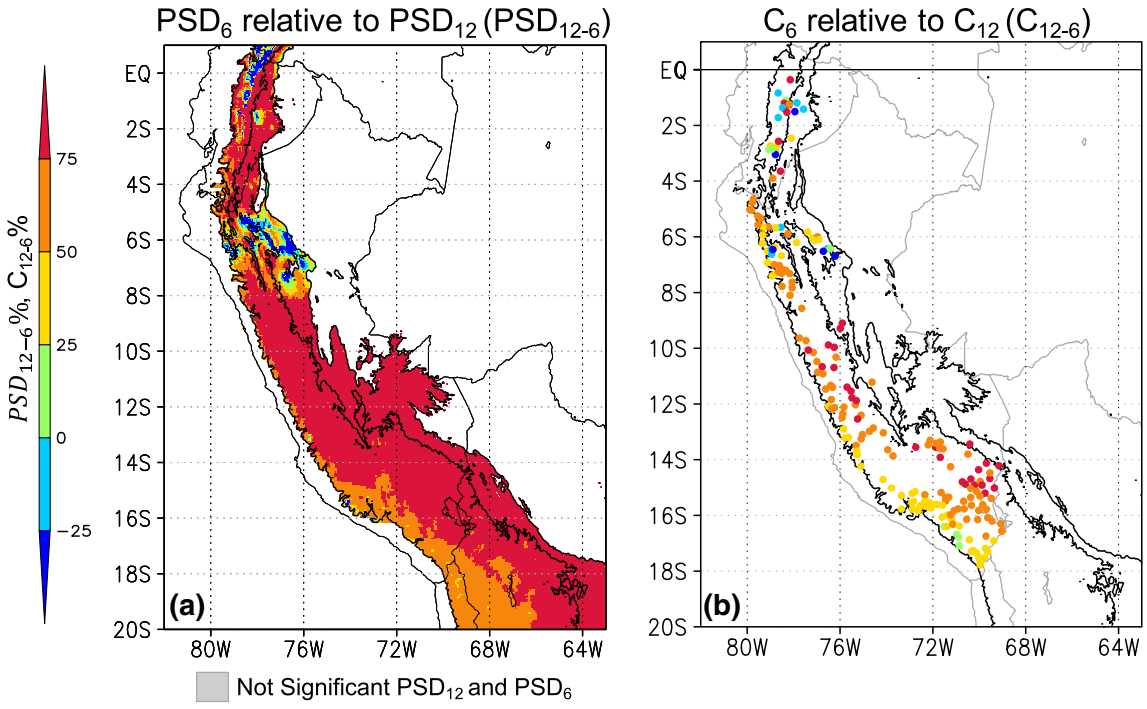

Fig. 2 **a** Relative difference between PSD_{12} and PSD_6 (PSD_{12-6}; shaded) using Eq. 3 and CHIRPS data set. **b** Relative difference between C_{12} and C_6 (C_{12-6}) estimated by using Eqs. 4, 5 and 6 and in-situ precipitation of 206 rain-gauge stations located in Peru and Ecuador. Topography contours (black solid lines) in **a**, **b** are the same as in Fig. 1

present missing values. Due to this fact, the computation of the power spectral density was not possible with the in-situ precipitation. Instead, we used the harmonic analysis in order to calculate the amplitude of the harmonic (C_k) at 6 (bimodal) and 12 (unimodal) months. In order to calculate the amplitude, first we used the expression:

$$H_k(t) = A_k \times cos\left(2 \times \pi \times \frac{t}{k}\right) + B_k \times sin\left(2 \times \pi \times \frac{t}{k}\right) + Ct \quad (4)$$

where H_k is the temporal series of the harmonic with a period k. We only calculated the harmonics with a period of 6 and 12 months. A_k and B_k are constants that modulate the cosine and sine functions at a period k, respectively. Ct is a constant value. t is the sequence of time, and in this study t starts at 1 and finishes at m, where m is the product of the numbers of years by 12. Then, the right hand of Eq. 4 was used in a regression analysis together with the time series of precipitation of each rain-gauge station in order to obtain the coefficients A_k and B_k. Finally, C_k is calculated using the following equation:

$$C_k^2 = A_k^2 + B_k^2 \quad (5)$$

The relative difference between the amplitudes at 6 and 12 months (C_{12-6}) is calculated following :

$$C_{12-6} = \frac{C_{12} - C_6}{C_{12}} \times 100 \quad (6)$$

As for PSD_{12-6}, negative values of C_{12-6} indicate that the bimodal precipitation regime is stronger than the unimodal one while positive values show the opposite. Contrary to the PSD analysis, the harmonic analysis could be influenced by non-recurring events that appear once in a short period of time.

3 Refining the characterization of the precipitation regimes over the tropical Andes

3.1 Unimodal and bimodal annual precipitation regimes

Figure 2a shows the spatial distribution of PSD_{12-6} and we observed that most of the tropical Andes present a unimodal regime of precipitation on seasonal time scales ($PSD_{12-6}\% > 0\%$). However, there are two regions in which the bimodal regime predominates ($PSD_{12-6}\% < 0\%$). One is located between 8°S and 5°S, and the other one is in the upper-elevation Andes between 1°S–1°N.

The spatial distribution of C_{12-6} also shows similar characteristics to PSD_{12-6} (Fig. 2b). A predominance of a unimodal precipitation regime is observed south of 8°S, but the values of C_{12-6} are smaller than the values of PSD_{12-6}. Low values of C_{12-6} in comparison to PSD_{12-6} could be explained by an overestimation of C_6 since the harmonic analysis could be influenced by non-recurring events. For instance, precipitation in the October–November period for three years could influence the amplitude of the C_6.

Over the region between 8°S and 5°S in zones where PSD_{12-6} is negative, rain-gauge stations show negative values of C_{12-6}. This is also observed north of 5°S, where the density of rain-gauge stations is still lower.

As Fig. 2a suggests, we could divide our zone of study in three regions: the southern tropical (20°S–8°S) and equatorial (5°S–1°N) Andes, which are characterized by a dominant unimodal precipitation regime on seasonal time scales, and a transition zone where a bimodal variability is well observed between 8°S–5°S. Using the precipitation in these three identified regions, we will analyze the principal modes of precipitation in the tropical Andes on seasonal and interannual time scales.

3.2 Principal rainfall modes on seasonal and interannual time scales

An EOF analysis is performed on the precipitation in each region with the aim of identifying their dominant spatio-temporal precipitation variability on seasonal and interannual time scales (see Data and Method for more details). Figure 3 shows the EOF (spatial pattern) in terms of correlation between the first principal component (PC) of each region and the precipitation field from CHIRPS over the tropical Andes. We refer to the first PC in the southern tropical Andes as PCS1, for the transition zone as PCT1 and for the equatorial Andes as PCE1. A correlation analysis was also performed between the first PC of each identified region (PCS1, PCE1 and PCT1) and the in-situ precipitation from rain-gauge stations located in the Peruvian and Ecuadorian Andes (Figure S1).

The first spatial mode in the southern tropical Andes (EOFS1; Fig. 3a) explains 78% of the total precipitation variance in Andean regions south of 8°S. High EOFS1 values ($r > 0.7$; p-value < 0.01) in Fig. 3a indicate that this region is strongly influenced by a common mode of rainfall variability. In addition, in-situ precipitation from rain-gauge stations located in the southern tropical Andes shows significant correlation values with PCS1 (p-value < 0.05; Figure S1).

The first principal mode of the transition zone (EOFT1; Fig. 3b) explains 71% of the total precipitation variance in this region. As expected, high values of EOFT1 indicates that precipitation over the transition zone is well represented by this spatial pattern ($r > 0.7$; p-value < 0.01). Furthermore, high EOFT1 values are observed over regions near the northern and southern boundaries of the transition zone ($r > 0.7$, p-value < 0.01), indicating that the transition zone shares a similar

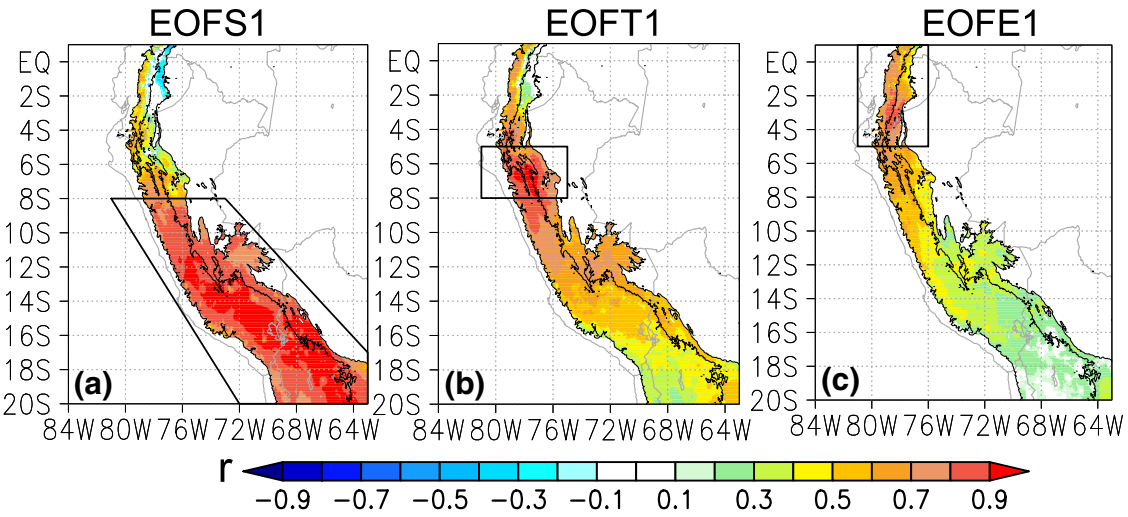

Fig. 3 First principal spatial mode (EOF) for the **a** southern tropical Andes (EOFS1), **b** transition zone (EOFT1) and **c** equatorial Andes (EOFE1). The zone where the EOF analysis is applied is enclosed by a polygon with black solid edge in **a**–**c**. Only correlation coefficients with p<0.01 are displayed. Topography contours (black solid lines) in **a**–**c** are the same as in Fig. 1. The seasonal and interannual variability for the associated time series of each EOF (PCs) are shown in Figs. 4 and 7, respectively

precipitation variability with some regions in the southern tropical and equatorial Andes. Using rain-gauge stations, we observe that PCT1 is significantly correlated with in-situ precipitation over the transition zone (p-value < 0.05; Figure S1).

Over the equatorial Andes the leading mode of precipitation variability explains 52% of the total variance (EOFE1; Fig. 3c). This smaller percentage, in comparison with EOFS1 (78%) and EOFT1 (71%), indicates that the equatorial Andes are characterized by a more complex spatio-temporal rainfall variability than the two other zones. In addition, low values of EOFT1 over the the eastern Andean slopes between 1°S–1°N highlight the existence of other modes of precipitation variability in this region, but they are less dominant than EOFE1. The correlation with in-situ precipitation shows that most of the rain-gauge stations located in the equatorial Andes display significant correlation values with PCE1, especially with rain-gauge stations situated above 2000 m.a.s.l (p-value<0.05; Figure S1). With the aim of analyzing if region 1°S–1°N is influencing our results, an EOF analysis was computed between 5°S and 1°N. The spatial pattern of the main mode of precipitation in the region 5°S–1°S is similar to EOFE1 (not shown); indeed, their principal components have a correlation coefficient of 0.98 with a p-value<0.05.

4 Seasonal precipitation variability in the tropical Andes and its associated atmospheric circulation

The temporal time series associated with the primary EOF calculated by each identified region, named principal components (PCS1, PCT1 and PCE1; not shown), are analyzed in this section. The atmospheric mechanisms associated with the seasonal variability of each PC are also analyzed in this section.

4.1 Principal precipitation regimes in the tropical Andes

The boxplot diagrams of the annual values of PCS1 (Fig. 4a), PCT1 (Fig. 4b) and PCE1 (Fig. 4c) indicate that precipitation in the southern tropical and equatorial Andes (Fig. 4a, c) follows a unimodal annual regime, while the transition zone is represented by a bimodal one (Fig. 4b), which is in agreement with the results obtained from the power spectral density analysis in Sect. 3 (Fig. 2a).

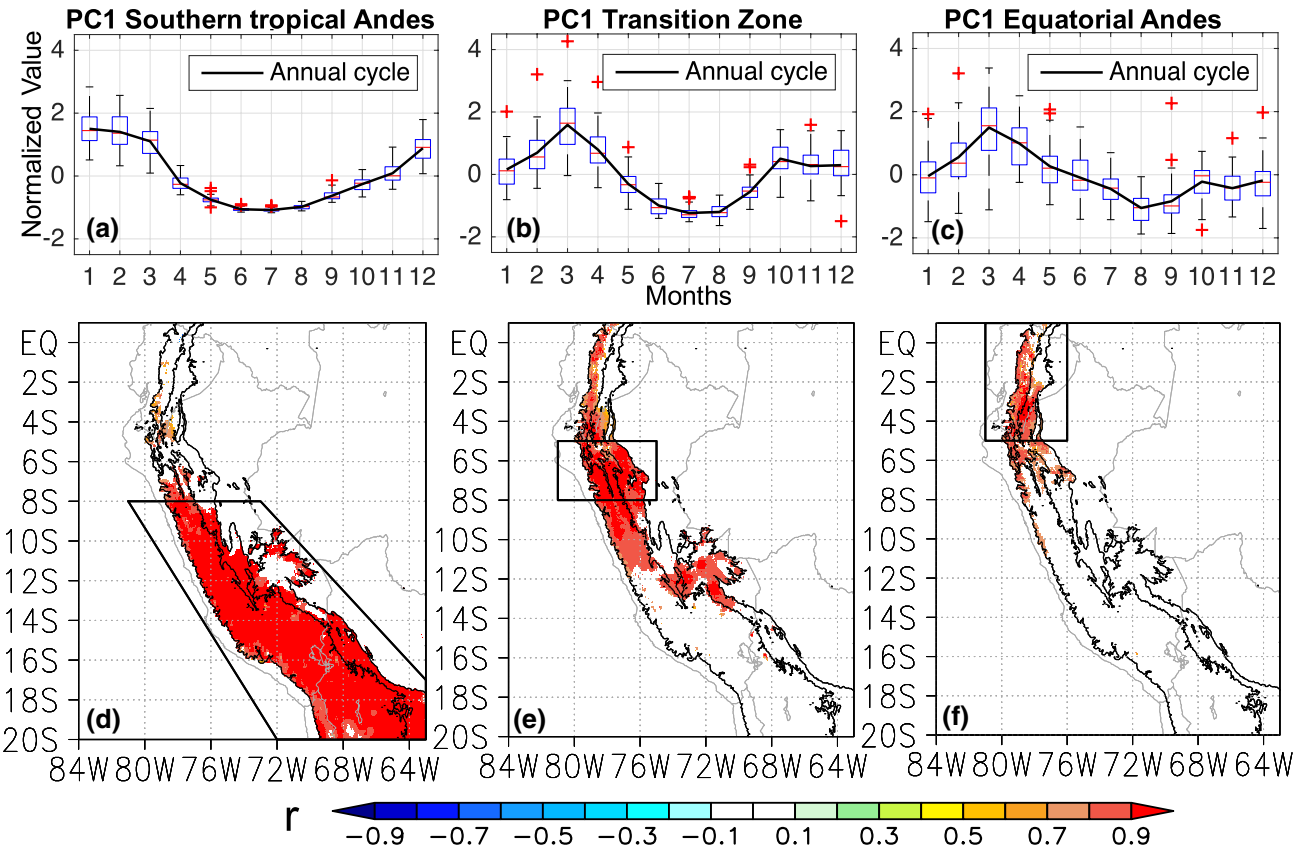

Fig. 4 Box-plot diagram of normalized annual values and the normalized annual cycle (black solid line) for the first principal components (PCs) of **a** the southern tropical Andes (PCS1), **b** transition zone (PCT1) and **c** equatorial Andes (PCE1). The percentile 25 (bottom blue line), 50 (red line) and 75 (upper blue line) are displayed. The outliers (red crosses) are values exceeding (below) the percentile 75 (25) plus (minus) 1.5 times the interquartile range. These limits are displayed in each box as the upper and lower horizontal black line. Correlation coefficients between the annual precipitation cycle at each grid point in the tropical Andes and the normalized annual cycle of **d** PCS1, **e** PCT1 and **f** PCE1. Only correlation coefficients with p-value < 0.05 are displayed. Topography contours (black solid lines) are similar to Fig. 1

As it is expected, the annual cycle of PCS1 shows that the southern tropical Andes are characterized by a wet season in the December–March period and a strong dry season in the June–August period (Fig. 4a). In addition, most of the interannual precipitation variability is observed during the wet period, with scarce extreme rainfall events during the dry season (Fig. 4a). Figure 4d shows a strong and significant (p-value < 0.05) correlation between the annual cycle of PCS1 and the annual cycle of precipitation over the southern tropical Andes.

In the equatorial Andes, the wet and dry periods are from February to April and from July to September (Fig. 4c), respectively. Moreover, there is a small increase in precipitation in October. Unlike the southern tropical Andes, the equatorial Andes show the presence of extreme rainfall events during the entire year, even during the dry period (Fig. 4c). The associated spatial correlation pattern between the annual cycle of PCT1 and the precipitation over the tropical Andes (Fig. 4f) shows significant (p-value<0.05) positive values in most of the equatorial Andes region, with the exception of the eastern Andean slopes between 2°S–1°N and the adjacent upper-elevation Andes, indicating that precipitation over these regions are modulated by a different type of seasonal variability.

The bimodal regime observed in the annual cycle of PCT1 presents two marked wet periods; one from February to April and another one from October to November (Fig. 4b), being the February–April wet season similar to the one observed in the equatorial Andes (Fig. 4c). On the other hand, a marked dry season is observed in the June–August period, similar to the one observed in the southern tropical Andes. The annual cycle of PCT1 is significantly correlated with the annual cycle of precipitation in the region 8°S–5°S (p-value < 0.05; Fig. 4e). Furthermore, the seasonal variability of PCT1 is significantly (p-value < 0.05) associated with the annual cycle of precipitation in some regions of the

northern and southern tropical Andes (Fig. 4e), confirming that this region acts as a transition zone between the unimodal regimes of the southern tropical and equatorial Andes.

4.2 Seasonal atmospheric circulation in the tropical Andes

To analyze the relationship between the seasonal precipitation in the tropical Andes and regional atmospheric circulation, we computed composites of climatological vertically integrated water vapor flux and vertically integrated water vapor for three (3) periods in the year (Fig. 5). The first one is from October to November (Fig. 5a), which is the beginning of the wet season in the southern tropical Andes (Fig. 4a), and the first wet season for the transition zone (Fig. 4b). The second is from December to February (Fig. 5b), and it is used to analyze the peak of the wet season in the southern tropical Andes (Fig. 4a). Finally, the period from March to April (Fig. 5c) is chosen to study the peak of precipitation in the transition zone and the equatorial Andes (Fig. 4b, c). Furthermore, the average precipitation during each period with respect to the mean annual value is also estimated at each grid point displayed in Fig. 5. To estimate these ratios, first the climatological annual cycle of precipitation is calculated at each grid point (12 months from January to December). Then, the climatological mean value for the period of study is estimated and divided by the mean

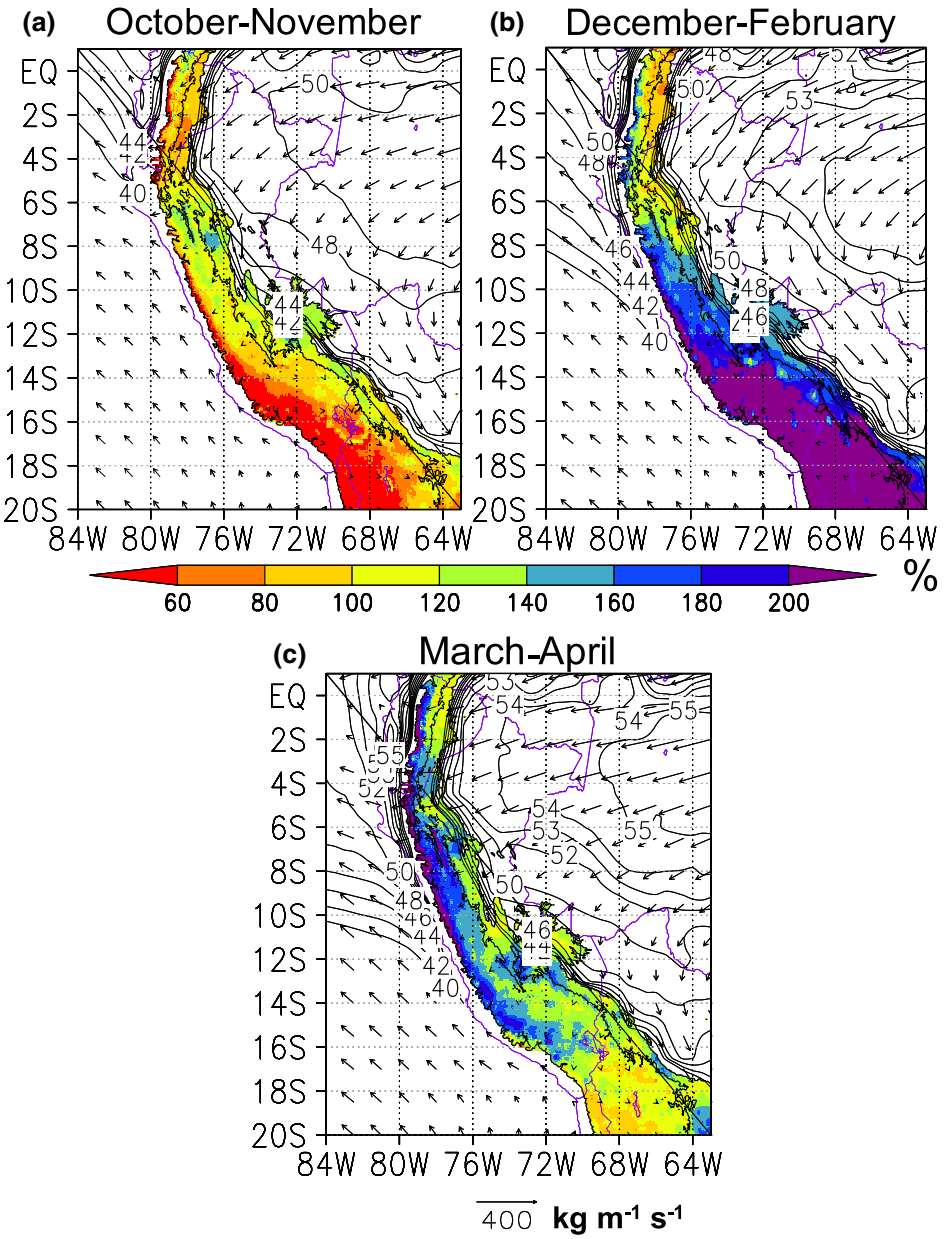

Fig. 5 Vertically integrated water vapor flux (vector), vertically integrated water vapor (contours, black thin line) and the ratio (shaded; %) between the climatological precipitation during the corresponding period and the mean value of the climatological period from January to December (annual cycle) at each grid point. Values grater (smaller) than 100% indicate that the precipitation during the analyzed period is above (below) to the mean value of the climatological annual cycle. The periods are: **a** October–November, **b** December–February, **c** March–April. Contours of vertically integrated water vapor start at 40 Kg m^{-2} with an increment of 2 Kg m^{-2} until 52 Kg m^{-2}. After 52 Kg m^{-2}, the increment is of 1 Kg m^{-2}. Topography contours (black solid line) are similar to Fig. 1

value of the climatological annual cycle. For instance, for the October–November period the climatological values of October and November are averaged and the result is divided by the mean value of the climatological period from January to December. Values grater (smaller) than 100% indicate that the precipitation during the October–November period is above (below) the mean value of the climatological annual cycle. The same method was applied to the other periods analyzed in this section.

The October–November period is marked by more precipitation with respect to the mean of the climatological annual cycle (> 100%) in the entire transition zone and the eastern slopes of the southern tropical Andes (Fig. 5a). The increased precipitation in the transition zone during this period is associated with a predominant westward component of the moisture flux in the equatorial zone and with a weak southward moisture flux along the eastern slope of the equatorial Andes.

The December–February period is characterized by an increase in precipitation over the entire southern tropical Andes, being more noticeable at upper-elevation regions, especially over the Altiplano (> 160%). During this period, a northward extension of the LLJ along the eastern Andean slopes and the western Amazon region can be observed (Fig. 5b). Over the eastern equatorial Pacific atmospheric humidity is enhanced with respect to the October–November period, which is related to the onset of the southward displacement of the eastern Pacific ITCZ.

In the March–April period precipitation decreases in the southern tropical Andes while the opposite is observed in the transition zone and the equatorial Andes, especially in the western upper-elevation zones of the Andes (> 140%; Fig. 5c). Figure 5c shows that the increased precipitation along the eastern flanks of the Andes north of 8°S is related to a combination of high atmospheric humidity values (≈ 53 kg m^{-2}) and an intensification of the westward moisture transport throughout the western Amazon north of 12°S. On the other hand, increased precipitation in the western upper-elevation Andean region north of 8°S is associated with high atmospheric humidity values over the eastern Pacific, probably related to the southward displacement of the ITCZ during this season as shown by Hastenrath (2002).

With the aim of evaluating the atmospheric circulation in the mid- and upper troposphere over the tropical Andes, we computed pressure–latitude cross-section composites of the horizontal wind and vertical motion from 1000 to 100 hPa along the tropical Andes (20°S–1°N; Fig. 6). We used the same periods as in Fig. 5, but we have also included the June–August period, which represents the dry season in the three identified regions. In the October–November period a baroclinic atmospheric structure is established over the tropical Andes, with westerly winds prevailing in the

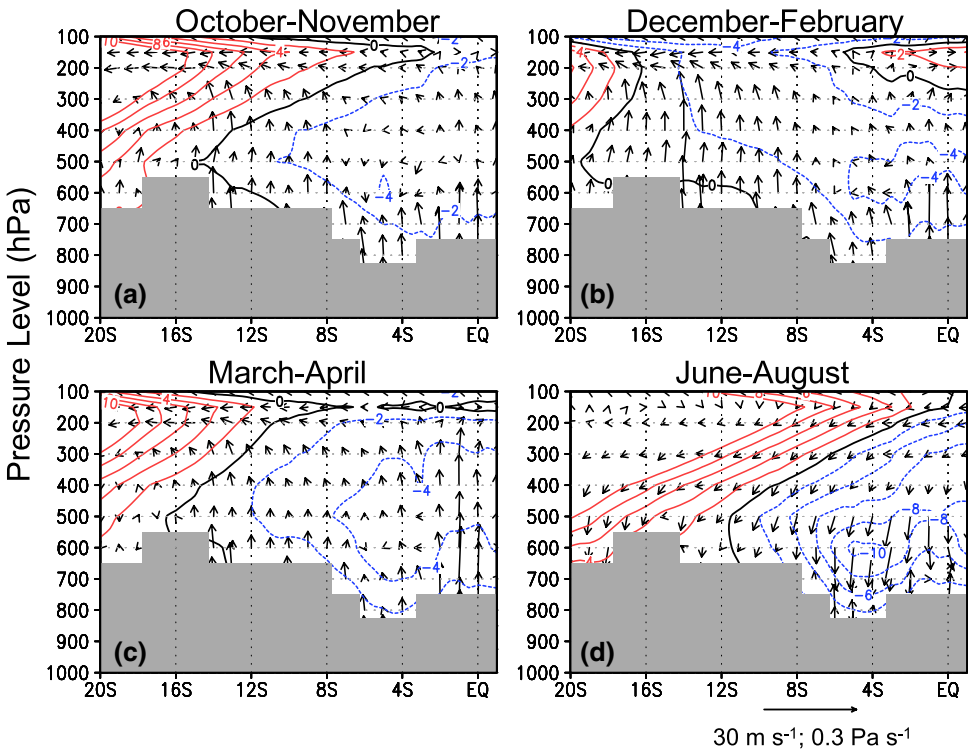

Fig. 6 Pressure–latitude cross-section of the climatological zonal wind (contours) and the climatological meridional-vertical wind (vectors) over the tropical Andes (20°S–1°N) for **a** October–November, **b** December–February, **c** March–April and **d** June–August. The zonal mean only takes in account wind data between 2000 m.a.s.l. in the western Andes slope and 350 m.a.s.l. in the eastern Andes slope. Red (blue) contours represent westerly (easterly) winds and the zero contour is displayed in black. The Andean topography is indicated with gray shading

upper troposphere and easterly winds in the mid-troposphere north of 10°S (Fig. 6a). Shallow convection is observed over Andean regions north of 8°S while weak ascending motion from 600 to 200 hPa is observed between 16°S–8°S.

In the December–February period, a barotropic atmospheric structure has been developed over the tropical Andes south of 6°S, with easterly winds dominating at all tropospheric levels (Fig. 6b). In the upper level, the zero line of zonal wind at 200 hPa indicates a Bolivian High (BH) centered at 16°S. Figure 6b also shows that the BH is associated with enhanced ascending motion over the southern tropical Andes. In contrast, the transition zone and the equatorial Andes display little mid-tropospheric ascending motion with westerly winds prevailing in the upper troposphere over these regions. Westerly winds in the upper troposphere over the eastern Pacific Ocean are related to an intensification of the Walker Cell in the equatorial Pacific during the austral summer (Schwendike et al. 2015).

During the March–April period, westerly winds dominate the upper and mid-troposphere over the southern tropical Andes, associated with low values of ascending motion (Fig. 6c). In contrast, the transition zone and the equatorial Andes are now characterized by enhanced ascending motion, especially the latter region (Fig. 6c). Moreover, the vertical atmospheric configuration observed north of 4°S in December–February has changed as westerly winds are weakened in the upper troposphere. Indeed, in March a core of easterly winds is seen over the equatorial Andes (not shown), suggesting a relationship between easterly winds at 200 hPa and deep convection over the equatorial Andes on seasonal time scales. No strong ascending motion is observed over the transition zone, neither in the March–April period nor in the October–November period.

In the dry period (June–August; Fig. 6d) a baroclinic atmospheric structure is established over the tropical Andes, with a thermal wind configuration and descending data sets over the entire Andean region (Fig. 6d). Between 6°S and 3°S easterly winds are channeled across the Andes along an orographic depression (Figs. 1b, 6d). Figure 1b also shows high values of precipitation in the eastern equatorial Andes during the June–August period. Strong westward winds in the equatorial zone at this time may lead to enhanced precipitation, but because of low atmospheric humidity and the large-scale subsidence, precipitation remains reduced in the upper-elevation zone of the equatorial Andes.

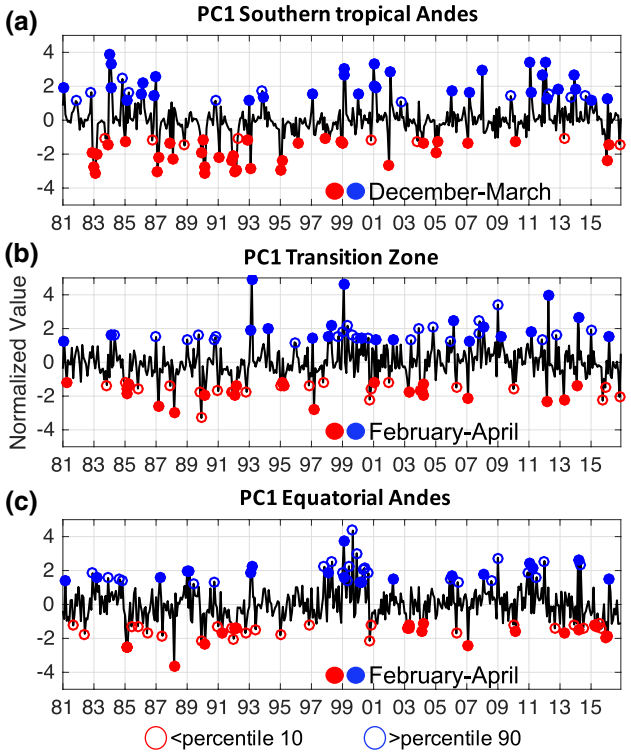

Fig. 7 **a** Normalized interannual monthly time series of the first principal components (PCs) for the southern tropical Andes (PCS1). Blue (red) circles highlight values above (below) percentile 90 (10). Filled circles are only for extreme values between December and March. **b**, **c** Similar to **a** but for the transition zone (PCT1) and the equatorial Andes (PCE1), respectively. Filled circles in **b**, **c** are for extreme values that occurred from February to April

5 Interannual rainfall variability in the tropical Andes and its associated atmospheric circulation

To study the interannual precipitation variability in the tropical Andes, the seasonal variability of PCS1, PCT1 and PCE1 was removed, by subtracting in each year the annual cycle of the respective time series. Next, each monthly interannual time series was normalized using its mean and its standard deviation values. Figure 7 shows the normalized interannual time series at monthly time step of PCS1 (Fig. 7a), PCT1 (Fig. 7b) and PCE1 (Fig. 7c).

At this time scale, the correlation coefficient between PCS1 and PCE1 (PCT1) is 0.13 (0.2), demonstrating that there is no linear relationship between precipitation over the Andes south and north of 8°S on interannual time scales. However, the correlation coefficient between PCE1 and PCT1 is 0.65 (p-value < 0.05), indicating that the transition zone and the equatorial Andes share a common signal on interannual time scales.

To analyze extreme monthly precipitation events in the entire tropical Andes on interannual time scales, the percentiles 90 (p90) and 10 (p10) are calculated for the entire interannual time series of each PC at monthly time step (Fig. 7a). Months where PC values fall above p90 and below p10 are selected and referred to as extreme precipitation events. For PCS1, 78% of all extreme events (86) occurred in months between December and March. For PCE1 (Fig. 7c) and PCT1 (Fig. 7b), we focused on the period from February to April, which is the wet season in both regions. In the equatorial Andes (PCE1), 41% of all the extreme events occur in this period, while in the transition zone (PCT1) the percentage is 48%. In the next subsections, extreme low and high monthly values of PCS1 that occurred from December to March are referred to as extreme monthly dry and wet events in the southern tropical Andes. The same nomenclature is used for the transition zone and the equatorial Andes for low and high monthly PCs values in each region between February and April.

5.1 Atmospheric circulation associated with precipitation in the southern tropical Andes

Composite analysis of precipitation anomalies and vertically integrated water vapor flux anomalies are calculated considering extreme monthly dry (Fig. 8a) and wet (Fig. 8b) events in the southern tropical Andes. Extreme monthly dry events show strong negatives anomalies of precipitation over the Altiplano and the Peruvian hotspot regions. These anomalies are accompanied by an anomalous southerly moisture flux along the eastern Andean slopes north of 10°S, indicative of decreased southward humidity transport from the equator. On a regional scale, significant negative precipitation anomalies are observed over equatorial South America (SA), probably related to significant westerly moisture flux anomalies that indicate reduced moisture transport from the equatorial Atlantic Ocean towards the continent (Fig. 8a). Significative positive anomalies of rainfall in eastern SA, coinciding with the continental region of the South Atlantic Convergence Zone (SACZ), and a significant cyclonic anomaly of moisture flux suggest moisture convergence in this zone.

The opposite spatial distribution of precipitation and moisture flux anomalies are observed during extreme monthly wet events (Fig. 8b), but with some differences. While no significant relationship between precipitation anomalies in the southern tropical Andes and anomalous southward humidity transport over the eastern Andean slopes north of 15°S is observed, significant anomalous westward moisture flux occurs between 10°S and 2.5°S over SA, indicative of enhanced humidity transport from the southern tropical Atlantic towards the continent. Furthermore, the equatorial SA rainfall signal is weaker than for extreme monthly dry events.

With the aim of analyzing the regional anomalies of convection, we computed a cross section of meridional humidity transport and zonal-vertical wind anomalies from 1000 to 100 hPa at 12°S for extreme monthly dry (Fig. 8c) and wet events (Fig. 8d). Extreme monthly dry (wet) events are significantly associated with weak (strong) ascending motion between 600–300 hPa over the Andes and western Amazon (Fig. 8c, d). Moreover, southward humidity transport in mid-tropospheric levels (700–500 hPa) appears to be limited by anomalous subsidence, while deep convection favors it.

A cross-section of mean zonal wind and mean vertical-meridional wind, computed for the tropical Andes from 1000 to 100 hPa for extreme monthly wet events (Fig. 8f), shows significant easterly winds dominating the upper troposphere between 20°S–8°S, which indicate a strengthening of the northern branch of the BH during wet events. This is also observed in Fig. 9b. Figure 8f shows that the center of the BH is located at 19°S, and it is accompanied by strong ascending motion all the way to 8°S. In contrast, extreme monthly dry events show significant westerly winds at upper levels north of 20°S (Fig. 8e), which indicate the absence of the Bolivian High as observed in Fig. 9a, and are accompanied by a weakened ascending motion over the southern tropical Andes (Fig. 8e).

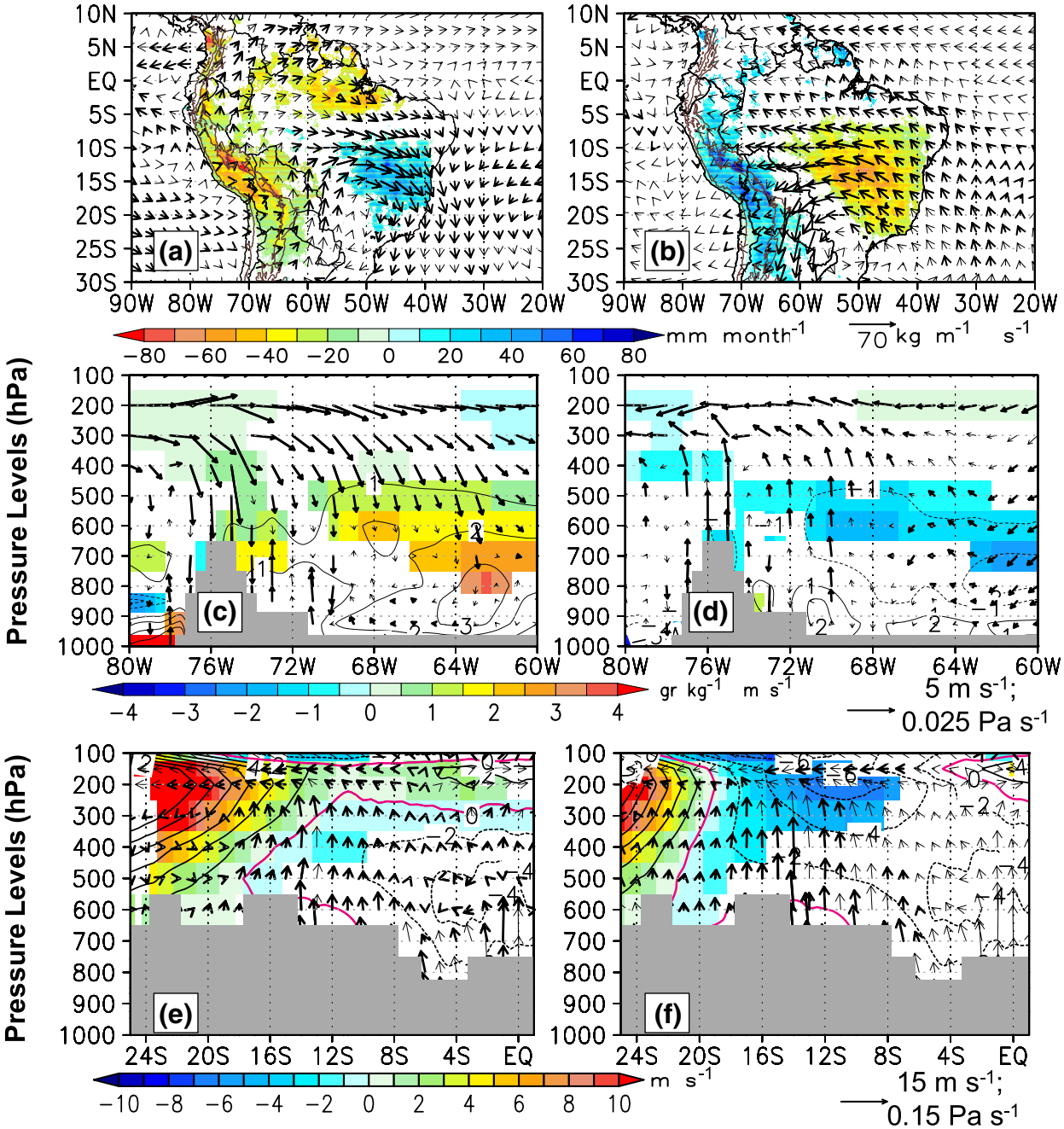

Fig. 8 **a** Composite for CHIRPS precipitation (shaded) and vertically integrated water vapor flux (vectors) anomalies considering dry events from December to March (DJFM) in the southern tropical Andes (PCS1). Only significant precipitation anomalies are shown and bold vectors represent significant meridional or zonal vertically integrated water vapor flux anomalies. Topography contours (black bold lines) are the same as in Fig. 1. **c** Pressure-longitude cross section at 12°S for anomalies of meridional humidity transport (contours; q × v), and zonal-vertical wind velocity (vectors) for dry DJFM events in the southern tropical Andes. Positive (negative) meridional moisture transport anomalies are represented by solid (dashed) lines and only significant values are shaded. Bold vectors represent significant vertical or zonal wind anomalies. Andes profile at 12°S is shown in gray. **e** Pressure–latitude cross section of mean zonal wind (contours) and mean meridional-vertical wind (vectors) averaged over the tropical Andes for dry DJFM events in the southern tropical Andes. The zonal mean only takes in account wind data between 2000 m.a.s.l. on the western Andes slope and 350 m.a.s.l. on the eastern Andes slope. Positive (negative) mean zonal winds values are drawn by solid (dashed) lines and only grid points with significant anomalies are shaded. Bold vectors represent significant meridional or vertical winds. Average zonal profile of the Andes in shown in gray. **b**, **d**, **f** similar to **a**, **c**, **e**, respectively, but for wet DJFM events

5.2 Atmospheric circulation associated with precipitation in the equatorial Andes

Composite analysis of precipitation and moisture flux anomalies are calculated to analyze the regional atmospheric circulation associated with extreme monthly dry (Fig. 10a) and wet (Fig. 10b) events in the equatorial Andes. Extreme monthly dry events are characterized by a significant deficit of precipitation over the entire region (5°S–1°N), with strong anomalies along the eastern Andean slopes. Significant negative anomalies are also observed in the southern tropical Andes between 6°S –15°S and along the Ecuadorian and northern Peruvian coast (Fig. 10a). Significant anomalous easterly moisture flux is observed over the eastern Pacific during dry events, indicating reduced moisture flux toward the western South American coast. Furthermore, significant easterly anomalies of moisture flux are apparent over equatorial South America. The opposite spatial pattern of precipitation and moisture flux anomalies is observed during extreme monthly wet events (Fig. 10b), but no significant moisture flux anomalies are found over equatorial South America, suggesting that extreme monthly wet events may be more closely associated with the variability of the atmospheric circulation over the eastern Pacific.

A cross-section at the Equator from 1000–100 hPa including anomalies of meridional humidity transport and anomalies of zonal-vertical wind for extreme monthly dry events (Fig. 10c) shows significant anomalous subsidence over the eastern Pacific, while anomalous upward motion is observed in the central Pacific (160°E–160°W). Furthermore, Fig. 10c also displays significant easterly wind anomalies in low and mid-tropospheric levels over the eastern equatorial Pacific. This is indicative of an intensification of the Walker Cell associated with an eastward displacement of the convection in the central Pacific (180°W –160°W). A significant increase in northward and westward humidity transport at low levels over the eastern Pacific indicates reduced moisture convergence along the western Andes (Fig. 10c), thereby limiting the potential for deep convection. Opposite atmospheric circulation patterns are observed during extreme monthly wet events (Fig. 10d), but no anomalous upward vertical motion is evident over the western Amazon. These results indicate that the weakening or strengthening of the Walker cell in the eastern Pacific plays an important role in the convection processes of the equatorial Andes by affecting moisture convergence and modulating atmospheric stability.

Calculating a cross section of the mean horizontal wind and mean vertical-meridional wind over all the tropical Andes from 1000 to 100 hPa for extreme monthly wet events (Fig. 10f), we noticed that easterly winds at 200 hPa are associated with deep convection north of 10°S. The barotropic atmospheric structure north of 10°S suggests that deep convection over the equatorial Andes is also maintained by moisture from the equatorial western Amazon (Fig. 10f). In contrast, extreme monthly dry events show intensified westerly winds at upper levels and a core of easterly winds at 600 hPa, accompanied by low values of ascending motion (Fig. 10e). Furthermore, it is interesting to notice that during extreme monthly wet events in the equatorial Andes, a Bolivian High is observed over the Peruvian Altiplano (Fig. 9d).

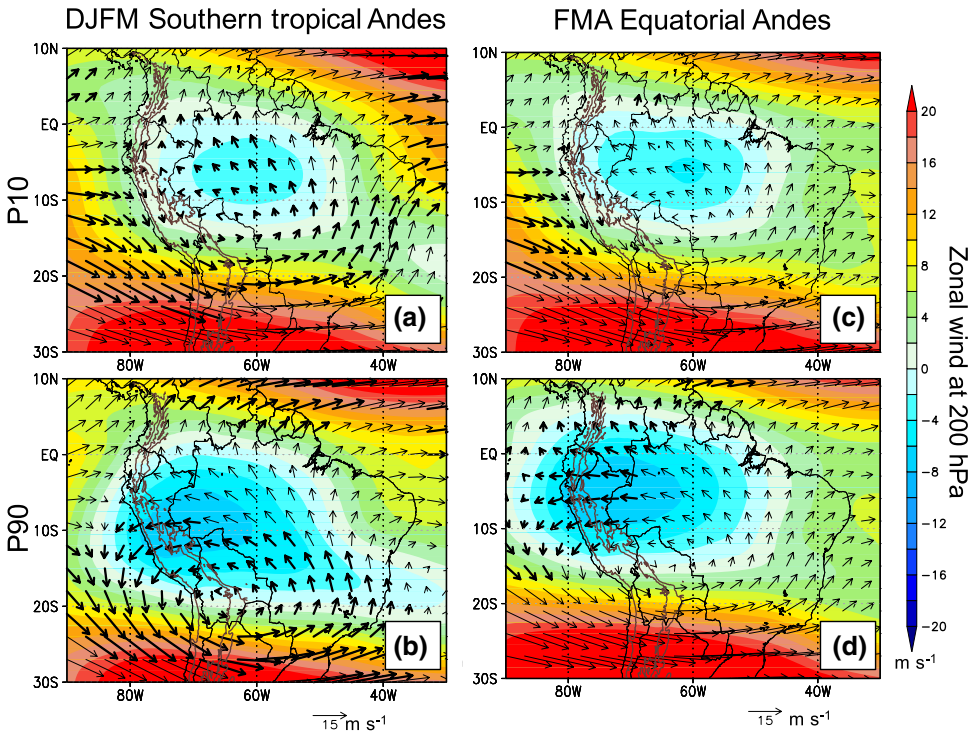

Fig. 9 Composites of mean zonal wind (shaded) and mean zonal-meridional wind component (vector) for **a** dry and **b** wet events from December to March (DJFM) in the southern tropical Andes. Bold vectors represent significant zonal anomalies. **c**, **d** similar to **a**, **b**, respectively but for dry and wet events in the equatorial Andes from February to April (FMA). The p-value used is $p<0.05$. Topography contours (brown bold lines) are drawn as in Fig. 1

5.3 Atmospheric circulation associated with precipitation in the transition zone

The composite of precipitation and moisture flux anomalies during extreme monthly dry events (Fig. 11a) in the transition zone shows dry conditions in the tropical Andes from 15°S to 1°N, with large negative rainfall anomalies along the eastern slopes of the equatorial Andes. The Ecuadorian and the northern Peruvian coast also shows dry conditions, probably related to intensified moisture transport away from the coast towards the central Pacific (Fig. 11a). Furthermore, Fig. 11a also displays negative rainfall anomalies in the equatorial Amazon, associated with reduced humidity transport from the equatorial Atlantic towards the continent. Opposite conditions are observed for extreme monthly wet events (Fig. 11b), except that

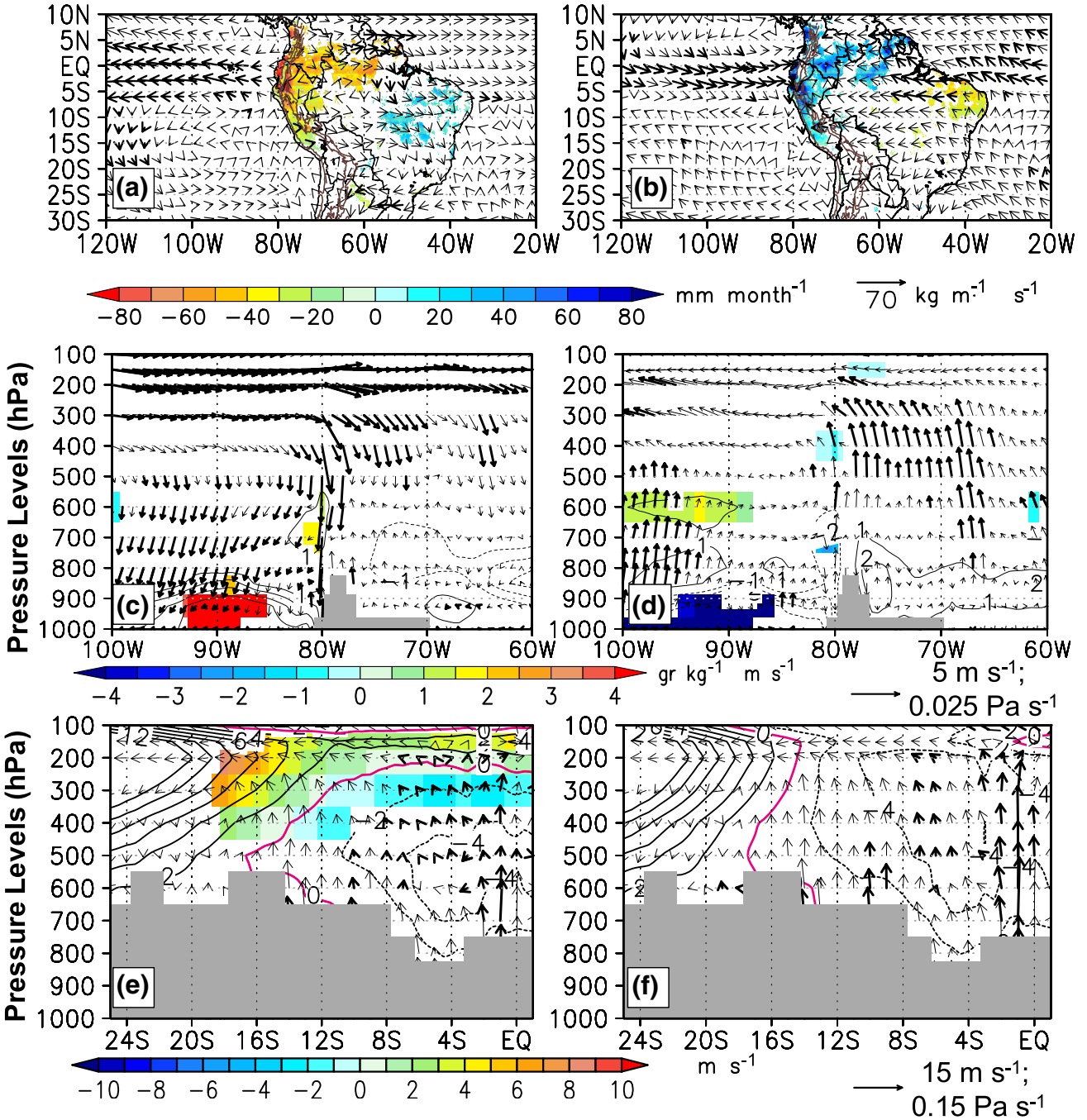

Fig. 10 The same as Fig. 8, but for dry **a**, **c**, **e** and wet **b**, **d**, **e** events that occurred in the equatorial Andes (PCE1) from February to April (FMA). The cross section in **c**, **d** was calculated at 0°N

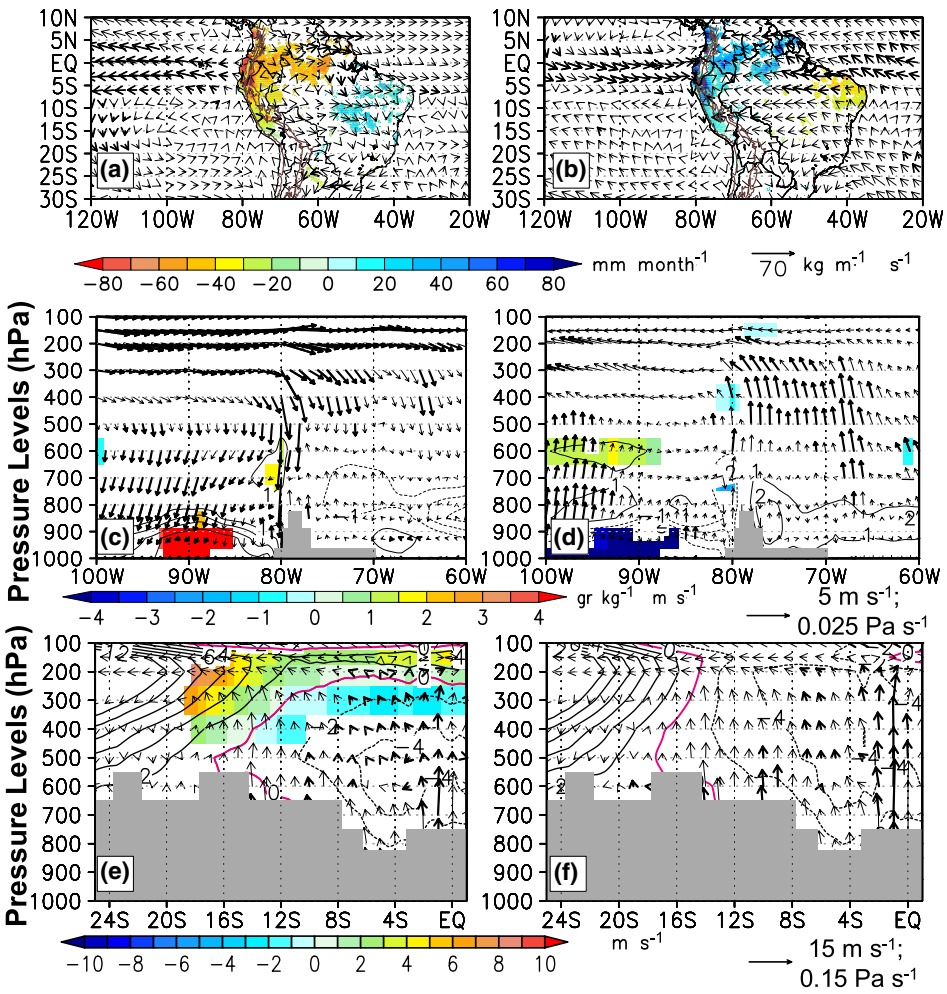

Fig. 11 The same as Fig. 8, but for dry **a**, **c**, **e** and wet **b**, **d**, **e** events that occurred in the transition zone (PCT1) from February to April (FMA). The cross section in **c**, **d** was calculated at 6°S

no significant precipitation anomalies are observed in the Ecuadorian Andes.

A cross-section at 6°S from 120°W to 60°W, in which anomalies of meridional humidity transport and anomalies of zonal-vertical wind from 1000–100 hPa are analyzed for extreme monthly dry (Fig. 11c) and wet events (Fig. 11d), reveals that dry events are characterized by anomalous subsidence over the eastern Pacific, suggesting a strengthening of the eastern branch of the Walker Cell (Fig. 11c), although not as strong as during dry events in the equatorial Andes (Fig. 10c). This could be the reason for similar spatial patterns of precipitation anomalies between the two zones (Figs. 10a, 11a). In contrast, wet events are related to enhanced upward motion over the western Amazon and less subsidence over the eastern Pacific (Fig. 11d).

Another important characteristic of extreme monthly wet events in the transition zone is the lack of a significant influence of zonal wind anomalies at 200 hPa. The composite of mean horizontal wind and vertical motion over the entire tropical Andes from 1000–100 hPa for wet events (Fig. 11f) confirms that zonal winds in the mid- and upper troposphere are not significantly related to precipitation in the transition zone. However, a barotropic atmospheric strcuture is observed with significant upward motion north of 8°S. We hypothesize that due to the reduced Andean topography in the transition zone when compared to the southern tropical or equatorial Andes, deep convection is not required to develop precipitation over the highest elevations of the transition zone. Opposite conditions are observed during extreme monthly dry events (Fig. 11e), in which significant westerly winds dominate the upper troposphere (200 hPa), demonstrating the intensification of the eastern branch of the Walker Cell.

5.4 Large-scale processes related to interannual rainfall variability in the tropical Andes

In this section we identify how the precipitation over the tropical Andes is related to SST and what atmospheric mechanisms may be involved in this process on a global scale. For this purpose, composites of SST and divergent wind (DW) anomalies at 200 hPa are calculated for extreme monthly dry and wet events in each of the three tropical Andean regions.

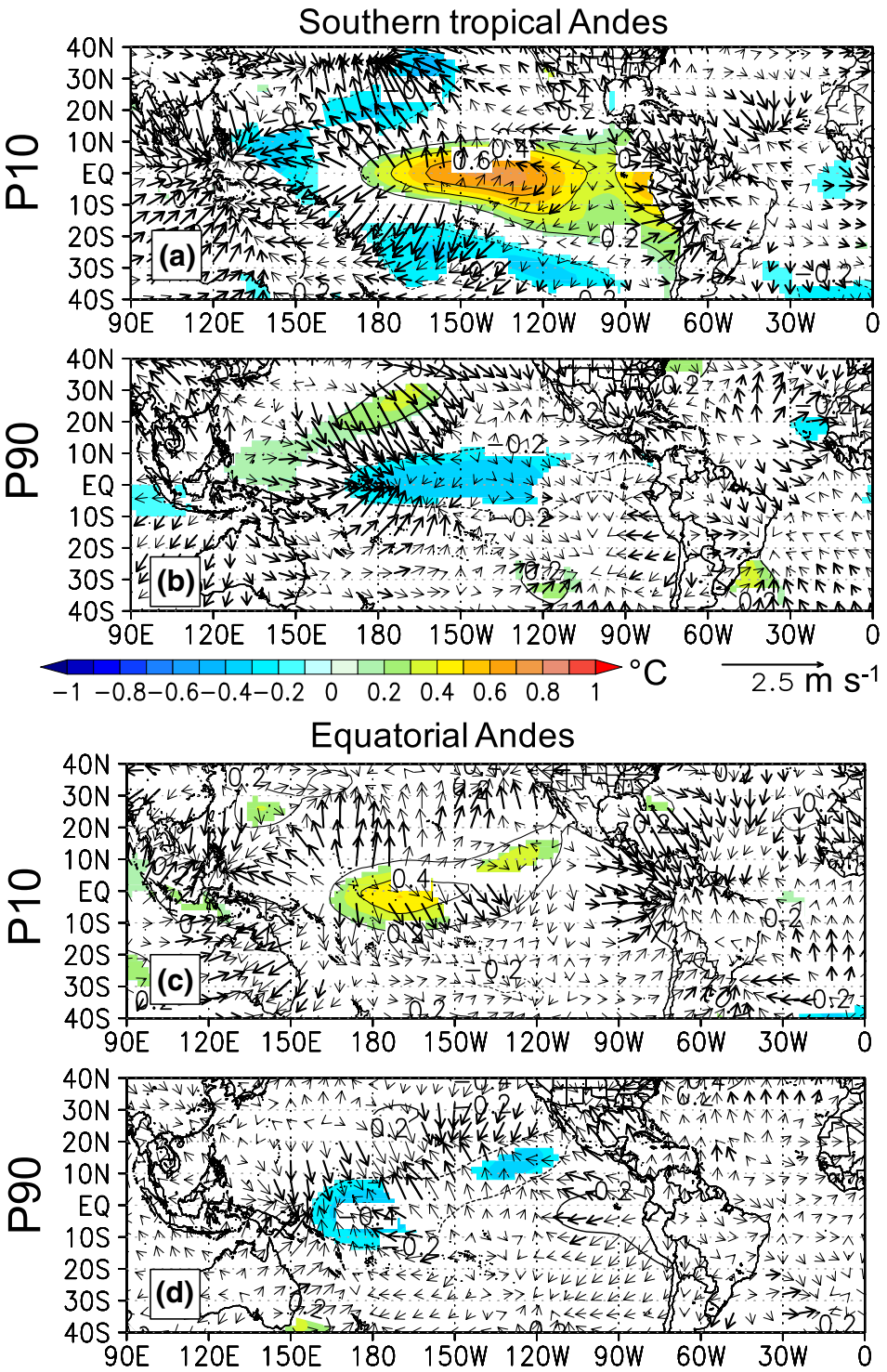

Fig. 12 Composite of sea surface temperature anomalies (SSTA; contours and shaded) and divergent wind anomalies (DW; vectors) at 200 hPa for **a** dry and **b** wet events from December to March (DJFM) in the southern tropical Andes. Positive (negative) SSTA are indicated by solid (dashed) lines and only significant anomalies are shaded. Bold vectors represent significant meridional or zonal anomalies of divergent wind. **c**, **d** similar to **a**, **b**, respectively, but for dry and wet events in the equatorial Andes from February to April (FMA). The p-value used is $p < 0.05$

Southern tropical Andes Extreme monthly dry events are characterized by a significant increase in SST in the central and eastern Pacific, while significant negative SST anomalies are observed in the western Pacific, the South Pacific Convergence Zone and the northern western tropical Pacific (Fig. 12a). This SST anomaly (SSTA) configuration is similar to the one observed during warm ENSO periods, which is related to significantly enhanced (weakened) convection over the central Pacific (western South America), observed in positive (negative) anomalies of divergent wind at 200 hPa (Fig. 12a, b). Garreaud and Aceituno (2001), demonstrated that warm ENSO years are characterized by an increase of temperature in the mid- and upper tropical troposphere that enhances the meridional

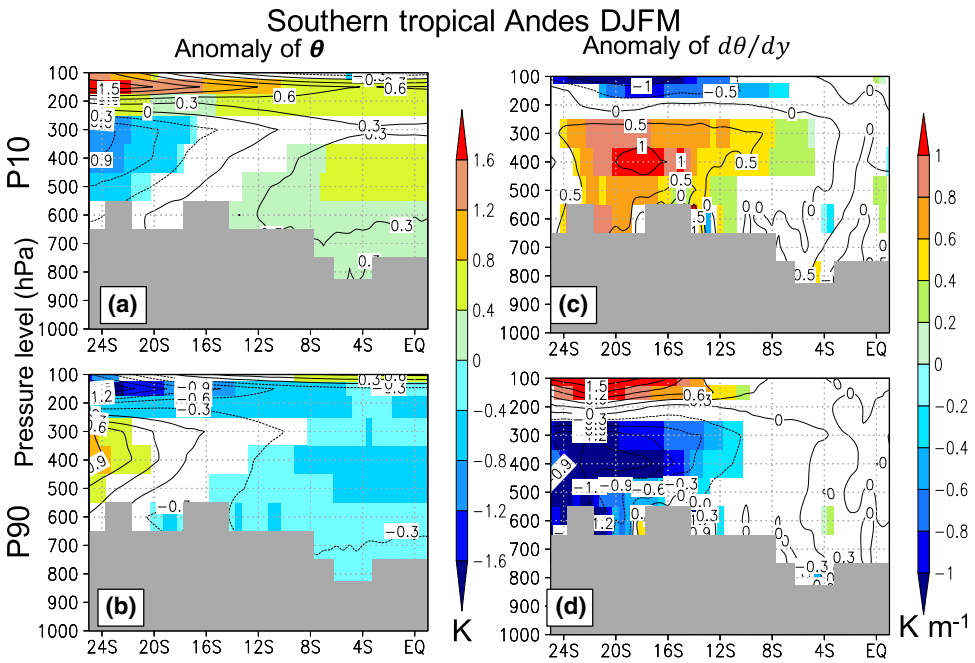

Fig. 13 Pressure–latitude cross-section of potential temperature (θ) anomalies averaged over the tropical Andes for **a** dry and **b** wet events from December to March (DJFM) in the southern tropical Andes. **c**, **d** As in **a**, **b**, respectively, but for the meridional potential temperature gradient. The zonal mean only takes in account θ between 2000 m.a.s.l. on the western Andes slope and 350 m.a.s.l. on the eastern Andes slope. Positive (negative) anomalies are indicated by solid (dashed) lines and only significant anomalies are shaded. The average zonal profile of the Andes is shown in gray shading

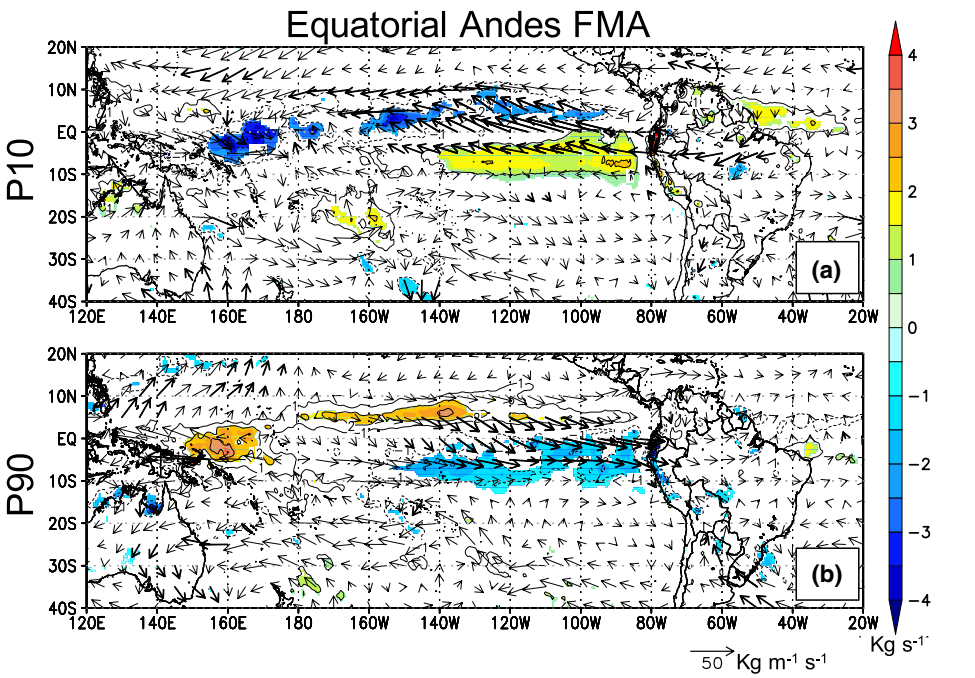

Fig. 14 Composite of divergence (contours and shaded) and horizontal component (vectors) of vertically-integrated moisture flux anomalies for **a** dry and **b** wet events between February and April (FMA) in the equatorial Andes. Positive (negative) anomalies of divergence are indicated by solid (dashed) lines and only significant anomalies are shaded. Bold vectors represent significant meridional or zonal vertically-integrated moisture flux anomalies. The p-value used is $p < 0.05$

temperature gradient between the tropics and the subtropics, producing westerly wind acceleration in the subtropics. These atmospheric features are present in the tropical Andes, where an increase of potential temperature in the northern Andes and a decrease in the southern Andes is observed (Fig. 13a), resulting in an increased meridional gradient of potential temperature with high values between 20°S–16°S at 400 hPa (Fig. 13c).

Extreme monthly wet events in the southern tropical Andes are associated with significant negative SSTA in the central Pacific and positive SSTA in the western Pacific (Fig. 12b). This SSTA configuration resembles the cold phase of ENSO but with weaker anomalies. The atmospheric configuration is opposite to the dry events, featuring a decrease of the meridional gradient, associated with cold

potential temperature anomalies in the northern Andes and warm anomalies in the southern tropical Andes (Fig. 13b, d).

Equatorial Andes Extreme monthly dry events do not show linkages to strong SSTA in the Pacific region, but significant and positive values are observed in the central-western Pacific (180°W–150°W; Fig. 12c). Significant DW anomalies at 200 hPa indicate decreased convective activity over equatorial South America (Fig. 12c), including the equatorial Andes, as shown in Fig. 10c, e. On the other hand, wet events show an SSTA dipole between the western (negative anomalies) and the eastern (positive anomalies) Pacific, but significant anomalies are found only in the western region. Moreover, significant DW anomalies at 200 hPa show that increased (decreased) convection occurs in the eastern (central-western) Pacific (Fig. 10d), influencing the enhanced upward motion over the equatorial Andes as displayed in Fig. 10d, f.

The configuration of the DW anomalies during extreme monthly dry events indicates an eastward displacement and an intensification of the Walker Cell, as shown in Fig. 10c, associated with warm SST anomalies in central-western Pacific. One of the possible atmospheric mechanisms related to this intensification is the northward displacement of the ITCZ as it is observed in the composite of integrated moisture flux divergence anomalies for extreme monthly dry events (Fig. 14a). Convergence anomalies, which are an indicator of precipitation, are displayed over almost the entire Pacific belt between 0°N–10°N. In contrast, the equatorial eastern Pacific shows significant divergence anomalies. These conditions could be intensified if cold SST anomalies dominate the eastern Pacific.

In contrast, cold SST anomalies in the western Pacific associated with warm SST anomalies in the eastern Pacific are associated with the southward displacement of the ITCZ, which is observed in the composite of integrated moisture flux divergence anomalies for extreme monthly wet events (Fig. 14b). Indeed, Fig. 14b shows significant convergence anomalies in the equatorial eastern Pacific, and suggests the development of deep convection over this region, which weakens the atmospheric stability over the eastern Pacific and as a consequence over the equatorial Andes. Moreover, several studies have indicated that positive SST anomalies in the eastern Pacific could destabilize the atmosphere and trigger precipitation in this oceanic region and along the northern Peruvian coast (Jauregui and Takahashi 2017; Takahashi and Martínez 2017; Xie et al. 2018). Indeed, Takahashi and Martínez (2017) suggested that cold SST in the central-western Pacific decreases the temperature in the mid- and upper tropical troposphere, creating the environment to trigger deep convection, while warm SST in the eastern Pacific favor a southward displacement of the ITCZ which destabilizes the atmosphere over the northern Peruvian coast.

A similar analysis was performed for the transition zone but no significant SST anomalies were found (not shown). However, anomalies of DW at 200 hPa are similar to those over the equatorial Andes (not shown).

6 Discussion and conclusion

Using a statistical metric (PSD_{12-6}) and the high spatial resolution CHIRPS precipitation data set, we divided the tropical Andes into three regions: the southern tropical Andes (20°S–8°S), the equatorial Andes (5°S–1°N) and the transition zone (8°S–5°S). Moreover, the first principal components (PCs), resulting from the EOF analysis on the precipitation in each identified region, allow us to characterize the principal precipitation variability in each of these regions (PCS1: southern tropical Andes ; PCE1: equatorial Andes; PCT1: transition zone) on seasonal and interannual time scales.

The representability of CHIRPS precipitation in the tropical Andes has been analyzed in previous studies. Paccini et al. (2018) obtained similar results by characterizing the intraseasonal variability of precipitation over the western Amazon basin, which includes the eastern slopes of the equatorial and south tropical Andes, using CHIRPS and the interpolated HYBAM observed precipitation (HOP) data sets. Espinoza et al. (2018) demonstrated that the CHIRPS precipitation data set is also able to detect the recent positive trend in precipitation over the northwestern Amazon basin, which has been identified using HOP. These studies have shown that CHIRPS precipitation is a formidable data set for studying precipitation variability in the tropical Andes and Amazonia, but caution should be taken in the equatorial Andes, an area characterized by low density of rain-gauge stations and where few studies have been conducted to validate CHIRPS.

An important result of our analysis is the characterization of the bimodal annual regime of precipitation in the transition zone. Besides, we show that the two wet seasons in this region are associated with different atmospheric mechanisms, which has not been documented before. The wet season in the October–November period is related to the westward humidity transport from the equatorial Amazon, while the wet season in the February–April period is also associated with the climatological southward migration of the ITCZ.

As previous studies have shown, the southern tropical Andes exhibit a unimodal annual regime of precipitation. In this study we also show that the influence of the LLJ and the BH modulates the seasonal precipitation variability of the tropical Andes between 20°S–8°S.

On the other hand, despite specific zones showing a bimodal annual regime of precipitation, the equatorial Andes

exhibit a predominance of a unimodal rainfall regime with a wet season in the February–April period. Even if the spatial distribution of rain-gauge stations is not sufficiently dense, the in-situ precipitation in regions where rain-gauge stations are available shows a similar annual rainfall regime to the one calculated using CHIRPS. Furthermore, the analysis of the seasonal atmospheric circulation provides an explanation for a unimodal rainfall regime because atmospheric conditions in the October–November period are not sufficient to develop deep convection over the equatorial Andes. In contrast, the southerly location of the ITCZ in the eastern Pacific and the intensification of the westward humidity transport from the equatorial Amazon in the February–April period create favourable atmospheric conditions for the development of deep convection and high values of precipitation over the upper-elevation zones of the equatorial Andes. Nevertheless, the existence of a bimodal annual regime at specific locations over the equatorial Andes is an interesting topic to be addressed in the future.

For the interannual analysis, the first PC for each identified region was deseasonalized and the corresponding percentile 10 and 90 were calculated. Then for each PC, months holding PC values above (below) percentile 90 (10) were categorized as extreme monthly wet (dry) events. In addition, we only analyzed extreme monthly wet and dry events in the December–March period for the southern tropical Andes (PCS1), and in the February–April period for the transition zone (PCT1) and the equatorial Andes (PCE1).

The composite analysis of December–March extreme monthly dry and wet events in the southern tropical Andes demonstrates a significant relationship between the precipitation in the upper-elevation Andes and the eastern Andean slopes in regions south of 8°S. Likewise, we found a statistical relationship between the convection over the western Amazon/eastern slopes of the Andes and the position and the intensity of the BH on interannual time scales. This relation is likely due to the westward moisture transport from the western Amazon associated with the strength and position of the BH. Previous studies have shown that the convection in the central Amazon influences the position of the BH (Silva Dias et al. 1983; DeMaria 1985; Figueroa et al. 1995). However, Lenters and Cook (1997) showed that the strength of the BH is also related to the condensation in the central Andes. Thus, the role of convection in the western Amazon in determining the position and the strength of the BH as well as the precipitation over the Altiplano should be addressed in future studies. On a large-scale, we showed that the SST variability over the central Pacific influences dry and wet events in the southern tropical Andes, as many studies suggested (e.g. Vuille 1999; Garreaud et al. 2003; Vuille and Keimig 2004; Sulca et al. 2018; Rau et al. 2017).

An interesting outcome of this study is that Andean regions in the transition zone are not primarly influenced by the SST variability in the central Pacific, meaning that the Niño and Niña events are not the main factor influencing the interannual precipitation variability over the equatorial Andes. For instance, February–April extreme monthly wet events in the transition zone are related to an increased convection over equatorial Amazon while February–April extreme monthly dry events are related to an intensification of the eastern branch of the Walker Cell. This suggests that the interannual variability in the transition zone is mainly modulated by regional- to local-scale atmospheric conditions. Our results highlight the importance of understanding the development of local convection over the transition zone and its relationship with humidity transport from the Amazon, the eastern Pacific and their interaction with the orography in this region, which is characterized by the lowest altitudes of the tropical Andes.

A clear influence of atmospheric processes in the eastern Pacific region on the precipitation of the equatorial Andes is observed during the February–April period. We show that an anomalous southerly (northerly) position of the ITCZ enhances (inhibits) convection and precipitation over the equatorial Andes on interannual time scales. Xie et al. (2018) showed that the interannual meridional displacement of the ITCZ is an important source of variability of the eastern Pacific region during the February–April period, and this is not related to SST variability in the Niño 1+2 region. This could be a reason for the non-significant relationship between February–April precipitation and SST in the eastern Pacific. Therefore, studies regarding the mechanisms related to the displacement of the ITCZ in the eastern Pacific are essential to better understand the February–April precipitation variability of the equatorial Andes. Moreover, we observed that easterly winds at 200 hPa are also associated with deep convection in the upper-elevation regions in the equatorial Andes during the February–April period.

Finally, we are well aware that atmospheric processes that operate at higher (< 4 months) and lower frequencies (> 7 years) also affect the tropical Andes region. For instance, previous studies have shown that extratropical cold air incursions have an impact on the precipitation over the Altiplano and the western Amazon (Espinoza et al. 2012; Sicart et al. 2016; Hurley et al. 2016; Paccini et al. 2018). On the other hand, Segura et al. (2016) demonstrated that the precipitation over the northern Altiplano is characterized by a significant decadal variability. Therefore, future studies need to also focus on understanding the intraseasonal and decadal precipitation variability over the tropical Andes.

Acknowledgements The first author H. S. was funded by the IRD program LMI-GREATICE, IDEX grants of University Grenoble Alpes (UGA), the VASPAT project IDEX "IRS-Initiative de Recherche

Stratégique" of UGA (part of the ANR project ANR-15-IDEX-02), and PNICP-Peru funds through contract 397-PNICP-PIAP-2014. Authors from IGE acknowledge the support of the Labex OSUG@2020 (Investissements d'avenir - ANR10 LABX56). The authors are grateful to J. -E. Sicart and C. Obled for stimulating exchanges within the CYME team of IGE and to J. Ronchail and L. Li of IPSL for discussions held in the framework of H. Segura's PhD. thesis committee.

References

Bendix A, Bendix J (2006) Heavy rainfall episodes in Ecuador during El Niño events and associated regional atmospheric circulation and SST patterns. Adv Geosci 6:43–49

Bendix J, Lauer W (1992) Die Niederschlagsjahreszeiten in Ecuador und ihre klimadynamische Interpretation (Rainy seasons in ecuador and their climate-dynamic interpretation). Erdkunde 2(1992):118–134

Bretherton CS, Widmann M, Dymnikov VP, Wallace JM, Bladé I (1999) The effective number of spatial degrees of freedom of a time-varying field. J Clim 12(7):1990–2009

Campozano L, Célleri R, Trachte K, Bendix J, Samaniego E (2016) Rainfall and cloud dynamics in the Andes: a Southern Ecuador case study. Adv Meteorol 2016:3192765

Campozano L, Trachte K, Célleri R, Samaniego E, Bendix J, Albuja C, Mejia JF (2018) Climatology and teleconnections of mesoscale convective systems in an andean basin in southern ecuador: the case of the paute basin. Adv Meteorol 2018(July):1–13

Chavez SP, Takahashi K (2017) Orographic rainfall hot spots in the Andes-Amazon transition according to the TRMM precipitation radar and in situ data. J Geophys Res Atmos 122(11):5870–5882

Cramér H (1999) Mathematical methods of statistics. Princeton mathematical series. Princeton University Press, Princeton

Dee DP, Uppala SM, Simmons AJ, Berrisford P, Poli P, Kobayashi S, Andrae U, Balmaseda MA, Balsamo G, Bauer P, Bechtold P, Beljaars AC, van de Berg L, Bidlot J, Bormann N, Delsol C, Dragani R, Fuentes M, Geer AJ, Haimberger L, Healy SB, Hersbach H, Hólm EV, Isaksen L, Kållberg P, Köhler M, Matricardi M, Mcnally AP, Monge-Sanz BM, Morcrette JJ, Park BK, Peubey C, de Rosnay P, Tavolato C, Thépaut JN, Vitart F (2011) The ERA-Interim reanalysis: Configuration and performance of the data assimilation system. Q J R Meteorol Soc 137(656):553–597

DeMaria M (1985) Linear response of a stratified tropical atmosphere to convective forcing. J Atmos Sci 42(18):1944–1959

Espinoza JC, Chavez S, Ronchail J, Junquas C, Takahashi K, Lavado W (2015) Rainfall hotspots over the southern tropical Andes: spatial distribution, rainfall intensity, and relations with large-scale atmospheric circulation. Water Resour Res 51(5):3459–3475

Espinoza JC, Ronchail J, Guyot JL, Cochonneau G, Naziano F, Lavado W, De Oliveira E, Pombosa R, Vauchel P (2009) Spatio-temporal rainfall variability in the Amazon basin countries (Brazil, Peru, Bolivia, Colombia, and Ecuador). Int J Climatol 29(11):1574–1594

Espinoza JC, Ronchail J, Lengaigne M, Quispe N, Silva Y, Bettolli ML, Avalos G, Llacza A (2012) Revisiting wintertime cold air intrusions at the east of the Andes: propagating features from subtropical Argentina to Peruvian Amazon and relationship with large-scale circulation patterns. Clim Dyn 41(7–8):1983–2002

Espinoza JC, Ronchail J, Marengo J, Segura H (2018) Contrasting North South changes in Amazon wet-day and dry-day frequency and related atmospheric features (1981–2017). Clim Dyn. https://doi.org/10.1007/s00382-018-4462-2

Figueroa SN, Satyamurty P, Da Silva Dias PL (1995) Simulations of the summer circulation over the South American region with an Eta coordinate model. J Atmos Sci 52:1573–1584

Francou B, Vuille M, Favier V, Caceres B (2004) New evidence for an ENSO impact on low-latitude glaciers: Antizana 15, Andes of Ecuador, 0°28'S. J Geophys Res Atmos 109(18):1–17

Funk C, Peterson P, Landsfeld M, Pedreros D, Verdin J, Shukla S, Husak G, Rowland J, Harrison L, Hoell A, Michaelsen J (2015) The climate hazards infrared precipitation with stations-a new environmental record for monitoring extremes. Sci Data 2:150066

Garreaud R (1999) Multiscale analysis of the summertime precipitation over the Central Andes. Mon Weather Rev 127:901–921

Garreaud R, Aceituno P (2001) Interannual rainfall variability over the South American Altiplano. J Clim 14(1987):2779–2789

Garreaud R, Vuille M, Clement AC (2003) The climate of the Altiplano: observed current conditions and mechanisms of past changes. Palaeogeogr Palaeoclimatol Palaeoecol 194(1–3):5–22

Garreaud RD (2009) The Andes climate and weather. Adv Geosci 22:3–11

Garreaud RD, Vuille M, Compagnucci R, Marengo J (2009) Present-day South American climate. Palaeogeogr Palaeoclimatol Palaeoecol 281(3–4):180–195

Gilman D, Fuglister F, Mitchell J (1963) On the power Spectrum of "Red Noise". J Atmos Sci 20(2):182–184

Hastenrath S (2002) The intertropical convergence zone of the Eastern Pacific revisited. Int J Climatol 22(3):347–356

Horel JD, Hahmann AN, Geisler JE (1989) An investigation of the annual cycle of convective activity over the tropical Americas. J Clim 2(11):1388–1403

Houston J, Hartley AJ (2003) The central Andean west-slope rainshadow and its potential contribution to the origin of hyper-aridity in the Atacama Desert. Int J Climatol 23(12):1453–1464

Huang B, Banzon VF, Freeman E, Lawrimore J, Liu W, Peterson TC, Smith TM, Thorne PW, Woodruff SD, Zhang HM (2015) Extended reconstructed sea surface temperature version 4 (ERSSTv4) Part I: Upgrades and intercomparisons. J Clim 28(3):911–930

Hurley JV, Vuille M, Hardy DR (2016) Forward modeling of δ18O in Andean ice cores. Geophys Res Lett 43(15):8178–8188

Jauregui YR, Takahashi K (2017) Simple physical-empirical model of the precipitation distribution based on a tropical sea surface temperature threshold and the effects of climate change. Clim Dyn 50:1–21

Junquas C, Li L, Vera CS, Le Treut H, Takahashi K (2016) Influence of South America orography on summertime precipitation in Southeastern South America. Clim Dyn 47(9–10):3389–3390

Krishnamurti TN, Kanamitsu M, Koss WJ, Lee JD (1973) Tropical East–West circulations during the northern winter. J Atmos Sci 30(5):780–787

Lagos P, Silva Y, Nickl E, Mosquera K (2008) El Nino related precipitation variability in Peru. Adv Geosci 3:231–237

Laraque A, Ronchail J, Cochonneau G, Pombosa R, Guyot JL (2007) Heterogeneous distribution of rainfall and discharge regimes in the Ecuadorian Amazon Basin. J Hydrometeorol 8(6):1364–1381

Lavado W, Espinoza JC (2014) Impactos de El Niño y La Niña en las lluvias del Perú (1965–2007). Rev Bras Meteorol 29:171–182

Lenters JD, Cook KH (1997) On the origin of the bolivian high and related circulation features of the South American climate. J Atmos Sci 54(5):656–678

Lorenz EN (1956) Empirical orthogonal functions and statistical weather prediction. Scientific report/Massachusetts Institute of Technology. Statistical Forecasting Project, Massachusetts Institute of Technology, Department of Meteorology, Cambridge

Paccini L, Espinoza JC, Ronchail J, Segura H (2018) Intra-seasonal rainfall variability in the Amazon basin related to large-scale

circulation patterns: a focus on western AmazonAndes transition region. Int J Climatol 38(5):2386–2399
Rau P, Bourrel L, Labat D, Melo P, Dewitte B, Frappart F, Lavado W, Felipe O (2017) Regionalization of rainfall over the Peruvian Pacific slope and coast. Int J Climatol 37(1):143–158
Rollenbeck R, Bendix J (2011) Rainfall distribution in the Andes of southern Ecuador derived from blending weather radar data and meteorological field observations. Atmos Res 99(2):277–289
Schwendike J, Berry GJ, Reeder MJ, Jakob C, Govekar P, Wardle R (2015) Trends in the local Hadley and local Walker circulations. J Geophys Res 120(15):7599–7618
Segura H, Espinoza JC, Junquas C, Takahashi K (2016) Evidencing decadal and interdecadal hydroclimatic variability over the Central Andes. Environ Res Lett 11(9):094016
Sicart JE, Espinoza JC, Quéno L, Medina M (2016) Radiative properties of clouds over a tropical Bolivian glacier: seasonal variations and relationship with regional atmospheric circulation. Int J Climatol 36(8):3116–3128
Silva Dias PL, Schubert WH, DeMaria M (1983) Large-scale response of the tropical atmosphere to transient convection. J Atmos Sci 40(11):2689–2707
Sulca J, Takahashi K, Espinoza JC, Vuille M, Lavado-Casimiro W (2018) Impacts of different ENSO flavors and tropical Pacific convection variability (ITCZ, SPCZ) on austral summer rainfall in South America, with a focus on Peru. Int J Climatol 38(1):420–435
Takahashi K, Martínez AG (2017) The very strong coastal El Niño in 1925 in the far-eastern Pacific. Clim Dyn. https://doi.org/10.1007/s00382-017-3702-1
Tanaka HL, Ishizaki N, Kitoh A (2004) Trend and interannual variability of Walker, monsoon and Hadley circulations defined by velocity potential in the upper troposphere. Tellus Ser A Dyn Meteorol Oceanogr 56(3):250–269
Thomson DJ (1982) Spectrum estimation and harmonic analysis. Proc IEEE 70(9):1055–1096
Tobar V, Wyseure G (2018) Seasonal rainfall patterns classification, relationship to ENSO and rainfall trends in Ecuador. Int J Climatol 38(4):1808–1819
Vera C, Higgins W, Amador J, Ambrizzi T, Garreaud R, Gochis D, Gutzler D, Lettenmaier D, Marengo J, Mechoso CR, Nogues-Paegle J, Dias PLS, Zhang C (2006) Toward a unified view of the American monsoon systems. J Clim 19(20):4977–5000
Vicente-Serrano SM, Aguilar E, Martínez R, Martín-Hernández N, Azorin-Molina C, Sanchez-Lorenzo A, El Kenawy A, Tomás-Burguera M, Moran-Tejeda E, López-Moreno JI, Revuelto J, Beguería S, Nieto JJ, Drumond A, Gimeno L, Nieto R (2017) The complex influence of ENSO on droughts in Ecuador. Clim Dyn 48(1–2):405–427
Virji H (1981) A preliminary study of summertime tropospheric circulation patterns over South America estimated from cloud winds. Mon Weather Rev 109(3):599–610
Vuille M (1999) Atmospheric circulation over the Bolivian Altiplano during dry and wet periods and extreme phases of the southern oscillation. Int J Climatol 19:1579–1600
Vuille M, Bradley RS, Keimig F (2000) Climate variability in the andes of ecuador and its relation to tropical Pacific and Atlantic sea surface temperature anomalies. J Clim 13:2520–2535
Vuille M, Hardy DR, Braun C, Keimig F, Bradley RS (1998) Atmospheric circulation anomalies associated with 1996/1997 summer precipitation events on Sajama Ice Cap. Bolivia J Geophys Res 103(D10):11191
Vuille M, Kaser G, Juen I (2008) Glacier mass balance variability in the Cordillera Blanca, Peru and its relationship with climate and the large-scale circulation. Glob Planet Change 62(1–2):14–28
Vuille M, Keimig F (2004) Interannual variability of summertime convective cloudiness and precipitation in the central Andes derived from ISCCP-B3 data. J Clim 17:3334–3348
Xie SP, Peng Q, Kamae Y, Zheng XT, Tokinaga H, Wang D (2018) Eastern pacific ITCZ dipole and ENSO diversity. J Clim 31(11):4449–4462
Zhou J, Lau KM (1998) Does a monsoon climate exist over South America? J Clim 11(5):1020–1040